The EUMETSAT Network of Satellite Application Facilities

ROM SAF
Radio Occultation Meteorology

# ROM SAF CDOP-2

# Visiting Scientist Report 21:

## Investigation of methods for the determination of the PBL height from RO observations using ECMWF reanalysis data

**Feiqin Xie**

Danish Meteorological Institute (DMI)
European Centre for Medium-Range Weather Forecasts (ECMWF)
Institut d'Estudis Espacials de Catalunya (IEEC)
Met Office (METO)

Ref: SAF/ROM/DMI/REP/VS21/001
Version: 1.0
Date: 3/12 2014

## DOCUMENT AUTHOR TABLE

| | *Author(s)* | *Function* | *Date* | *Comment* |
|---|---|---|---|---|
| Prepared by: | Feiqin Xie | ROM SAF Visiting Scientist | 14/11/2014 | |
| Reviewed by (internal): | Stig Syndergaard | ROM SAF Design Coordinator | 20/11 2014 | |
| Approved by: | Kent B. Lauritsen | ROM SAF Project Manager | 3/12/2014 | |

## DOCUMENT CHANGE RECORD

| *Issue/Revision* | *Date* | *By* | *Description* |
|---|---|---|---|
| Draft 1 | 27/08/2014 | FX | First draft |
| Draft 2 | 19/11/2014 | FX | Second draft |
| 1.0 | 03/12/2014 | FX | Included final comments from SSY and KBL |
| | | | |
| | | | |

**VS Author**

This VS study was carried out by Dr. Feiqin Xie, Department of Physical & Environmental Sciences, Texas A&M University-Corpus Christi, Texas, USA;
Email: Feiqin.Xie@tamucc.edu

**VS Duration**

The VS study was performed during a six weeks visit to DMI (July – August 2013) and then July 2013 – November 2014 at the home institute of the candidate.

**ROM SAF**

The Radio Occultation Meteorology Satellite Application Facility (ROM SAF) is a decentralised processing center under EUMETSAT which is responsible for operational processing of GRAS radio occultation data from the Metop satellites and radio occultation (RO) data from other missions. The ROM SAF delivers bending angle, refractivity, temperature, pressure, and humidity profiles in near-real time and offline for NWP and climate users. The offline profiles are further processed into climate products consisting of gridded monthly zonal means of bending angle, refractivity, temperature, humidity, and geopotential heights together with error descriptions.

The ROM SAF also maintains the Radio Occultation Processing Package (ROPP), which contains software modules that will aid users wishing to process, quality-control and assimilate radio occultation data from any radio occultation mission into NWP and other models.

The ROM SAF Leading Entity is the Danish Meteorological Institute (DMI), with Cooperating Entities: i) European Centre for Medium-Range Weather Forecasts (ECMWF) in Reading, United Kingdom, ii) Institut D'Estudis Espacials de Catalunya (IEEC) in Barcelona, Spain, and iii) Met Office in Exeter, United Kingdom. To get access to our products or to read more about the ROM SAF please go to: http://www.romsaf.org.

**Intellectual Property Rights**

# List of Contents

# Executive Summary

The planetary boundary layer height (PBLH) is a fundamental parameter characterizing the vertical extent of atmospheric mixing near the surface. It is critical for understanding the PBL process and low cloud evolution and its feedback on the climate system, which remains a key challenge in weather and climate modeling. The PBL height is generally defined as the altitude of a transition layer where air temperature or humidity gradient are significant within the lowest 1-5 km above the surface. Numerous thermodynamic parameters, including temperature, humidity (specific/relative humidity) and the derived variables (e.g., potential/virtual potential temperature etc.) have been widely used to obtain PBL height. The high vertical resolution GPS radio occultation (RO) measurements offer additional physical parameters for PBLH sensing, including atmospheric refractivity, bending angle and dry temperature.

In this project, we investigate six different PBLHs derived from the conventional physical parameters and simulated GPS RO observables over global oceans by using one-year high-resolution ERA-interim global reanalysis. Given a vertical profile of a specific physical parameter, automatic algorithm is applied to derive the PBLH at each model grid by using the simple gradient method. The global PBLH seasonal climatologies for each parameter are derived and compared with particular focus on understanding the characteristics of the PBLHs derived from GPS RO observables.

Over the subtropical eastern oceans near the coast, minimum difference (<200 m) and high correlations (>0.7) among various PBLHs are found, where well-defined PBLH is marked by sharp temperature and moisture gradients. Discrepancy among PBLHs is most prominent over tropical and polar regions. Refractivity based PBLH is most consistent with that of bending angle. Refractivity and specific humidity gradients tend to be more sensitive to a shallow mixing layer (below ~800 m) over equatorial and subtropical trade-wind regions and result in systematically lower PBLHs than the relative humidity and dry temperature based PBLH. The dry temperature ($T_{dry}$) based PBLH is highly consistent/correlated with that of *RH* from tropics to mid-latitude but exhibits large discrepancy over dry polar region. The dry temperature is also capable of detecting the PBLH marked by a weak shallow inversion in dry polar winter season, when the humidity based PBLHs become unreliable. Various physical parameters exhibit very different sensitivity to temperature and/or humidity gradients used to define the PBLH, and results in systematical difference among PBLH retrievals. All three GPS RO observables are well suited for PBLH sensing but with distinct differences. The dry temperature could be the best for global PBLH monitoring for its wide applicability from moist tropics to dry polar region.

To develop PBLH product from GPS RO measurements requires further development of a robust algorithm that considers both the noise and vertical resolution in RO measurements. Both temporal and spatial sampling errors (mainly in meridional and vertical) also need to be quantified. Beyond the PBLH product, improving GPS RO retrieval inside PBL is necessary for deriving high-quality RO PBL profiles, which provide critical atmospheric vertical structures information for PBL studies.

# 1. Introduction

## 1.1 Purpose of Document

This document contains the results from a ROM SAF Visiting Scientist activity from July 2013 to November 2014. The objective is to use ECMWF reanalysis to study the difference in planetary boundary layer (PBL) height (PBLH) climatology derived from conventional physical parameters as well as the simulated GPS radio occultation (RO) observables over global oceans. Special focus is on the understanding and recommending GPS RO observable for PBLH measurements.

The document is organized as follows: the remainder of Chapter 1 provides motivation and background of the PBL study. Chapter 2 summarizes the ECMWF reanalysis data used in this study and the methods for simulating GPS RO observables and estimating PBLH with each physical parameter. Chapter 3 presents the PBL height climatology derived from both conventional parameters and the GPS RO observables. The difference and correlation among various PBLH definitions are examined. The PBL transect and vertical structures from selected regions are explored to understand the systematic PBLH differences. Finally, a summary and discussion of PBLH characteristics along with some recommendations for deriving GPS RO based PBLH are presented in Chapter 4.

## 1.2 Background on the Planetary Boundary Layer

The planetary boundary layer (PBL) is one of the key components of the weather and climate system that controls the exchanges of energy, mass and momentum between the earth's surface and the free troposphere (Garratt 1992). The PBLH is a crucial parameter in the PBL process, which measures the vertical scale of turbulent eddies and controls turbulent mixing, heat and moisture fluxes exchange among the PBL, the underlining surface and the free troposphere. The shallow depth (1~3 km) and frequent cloud presence in the PBL have been a great challenge for models to simulate and for satellite sensors to probe. Most of the current PBL observations are restricted to sparse radiosonde soundings and field campaigns. The limited spatial and temporal coverage of PBL observations hinder the understanding of complex PBL processes and leads to poor representation and prediction skills of the PBL and the associated low cloud formation in the climate and weather models (e.g., Duynkerke and Teixeira, 2001; Bretherton et al., 2004; Bony and Dufresne, 2005; Stephens, 2005; Soden and Held, 2006; Wyant et al., 2006; Clement et al., 2009). Continuously monitoring the global PBL vertical structures will provide a critical dataset to evaluate various PBL parameterization schemes through the diagnostic analysis and combat the related model uncertainty issues.

The PBL height (PBLH) generally refers to the altitude of a very thin transition layer (on the order of 10 m to a couple 100 m) where a large temperature inversion and/or a moisture gradient are located. Such a thin transition layer becomes a huge challenge for both global modeling and satellite observation, as it is difficult to resolve by the limited vertical resolutions in most global models and observing systems.

In practice, The PBLH is commonly defined as the altitude where air temperature or humidity gradient become most significant within the lowest 5 km atmosphere above the surface. Numerous thermodynamic parameters, including temperature, humidity (specific/relative humidity, $q$ and $RH$) and their derivable (e.g., potential/virtual potential temperature etc.) have been widely used to define the PBLH. The gradient method, i.e., identify the maximum (positive) or minimum (negative) gradient in temperature or humidity, can be easily applied to locate the PBLH.

As an active limb sounding technique, the GPS RO offers direct sounding of atmospheric thermodynamic structure with global coverage, high vertical resolution (~100-200 m) and all-weather sampling capability. The vertical profiles of the RO soundings can be easily used for PBLH detection with simple gradient method. It is worth noting, however, the GPS RO does not directly retrieve temperature and humidity profiles. The temperature and humidity retrieval in the moist lower troposphere requires the a-priori information from models and thus are not independent observables. Instead, the independent RO observables are non-conventional parameters such as atmospheric refractivity, bending angle and dry temperature, which could offer model-independent PBLH observations.

Recent studies have shown the feasibility of the RO technique to detect the PBLH (e.g., von Engeln et al 2005; Sokolovskiy et al., 2006; Sokolovskiy et al., 2007). Several studies have used RO refractivity profile to detect PBL height by locating the height of maximum refractivity gradient (MRG, most negative) in GPS RO profiles (e.g., Ao et al., 2008; Basha and Ratnam, 2009; Ao et al., 2012; Xie et al., 2012). A similar but slightly different definition is to find the point where the refractivity lapse rate changes the most (the "breakpoint") (Sokolovskiy et al., 2006, 2007; Guo et al., 2011). For a well-defined PBL, the PBLH derived from refractivity is consistent with other conventional parameters (Basha and Ratnam, 2009; Seidel et al., 2010; von Engeln and Teixeira, 2013). However, over regions with weaker vertical gradient (e.g. the deep convection zone), significant discrepancies of PBLHs exhibit in different PBL height definitions (Seidel et al., 2010; von Engeln and Teixeira, 2013).

A standard universal definition of global PBL height does not exist due to the large variation of PBL vertical structures as a result of various PBL physical processes (e.g., moisture, momentum, stability, clouds and mesoscale or synoptic perturbation). Seidel et al. (2010) reveal large discrepancy among various PBL height definitions based on detailed analysis of global radiosonde soundings, which, however, are restricted over land and represent limited horizontal scales of atmospheric conditions. It is important to further investigate the PBLH difference retrieved from various atmospheric parameters in a global perspective, especially over vast oceans where limited in-situ observations are available. In this project, special emphasis will be on the study of the difference between the GPS RO based PBLHs and the conventional parameters based PBLHs. This will allow a better interpretation of the PBLH derived from the GPS RO and provide guidance for their usage for model evaluation purpose. A list of conventional parameters (e.g., temperature, humidity) and GPSRO parameters are shown in Table 1.

To accomplish the objectives, we use the ECMWF global reanalysis: ERA-interim, which provides high-resolution, uniform-gridded atmospheric thermodynamic structures globally. Various types of PBL structures from moist tropics to the dry polar region can all be studied in one consistent dataset. The advantages and limitation of various PBLH

definitions can be assessed with regard to different PBL structures. Specifically, we will investigate how GPS RO based PBLHs resemble or differ from other conventional PBLH definitions.

Table 1. Conventional and GPS RO parameters used for PBL height definitions.

| | Parameters (Abbreviation) | Method | Abbreviation |
|---|---|---|---|
| Conventional | Temperature ($T$) | Maximum gradient (positive) | $PBLH_T$ |
| | Specific Humidity ($q$) | Minimum gradient (negative) | $PBLH_q$ |
| | Relative Humidity ($RH$) | Minimum gradient (negative) | $PBLH_{RH}$ |
| GPS RO | Refractivity ($N$) | Minimum gradient (negative) | $PBLH_N$ |
| | Dry temperature ($T_{dry}$) | Maximum gradient (positive) | $PBLH_{Tdry}$ |
| | Bending Angle ($\alpha$) | Minimum gradient (negative) | $PBLH_\alpha$ |

It is worth noting that even though the ERA-interim reanalysis assimilates a large amount of in-situ, airplane and satellite measurements, the improvement inside the PBL is still limited, mainly due to the lack of high-quality observations, especially over data-sparse regions. Therefore, it is expected that the reanalysis could have “uncertainty” or even bias in PBL vertical structures, which was revealed in several studies (e.g., Bretherton et al., 2004; Wyant et al., 2010; Xie et al., 2012). The major focus of this project is on the PBLH difference retrieved from various parameters, but not on evaluating the accuracy of the PBL structures. In this regard, the global reanalysis provides a consistent dataset of global PBL structures and is quite valuable for such a study.

# 2. Data and Method

In this section, a brief introduction of the GPS radio occultation (RO) sounding technique and the major observables will be presented. The ERA-interim (ERA-i) global reanalysis and the simulated RO observables from the reanalysis will be elaborated.

## 2.1 GPS RO observables

GPS RO senses the atmosphere using GPS radio signals that traverse the atmosphere as a moving receiver sets or rises behind the horizon relative to the transmitting satellite. The radio signal is refracted (bent) and its travel time is delayed due to the atmospheric medium. Strictly speaking, the propagation of the GPS signal through the atmosphere obeys Maxwell's equation in which the propagation medium (e.g., the Earth's atmosphere) is characterized by a three-dimensional spatial distribution of a complex and dispersive refractive index.

The GPS RO technique precisely measures the phase and amplitude of the GPS navigation signals that pass through the Earth's atmosphere. After the phases are calibrated to remove the GPS and LEO clock errors etc., a time series of excess phase at both GPS frequencies (e.g., L1 and L2) are derived. Then the atmospheric bending angle and therefore the vertical structure of atmospheric refractive index can be derived. The advent of open-loop tracking significantly reduces receiver tracking errors (e.g., Beyerle et al., 2006) and allows the GPS RO to probe deep into the moist lower troposphere (Sokolovskiy 2001; Ao et al., 2009) and make it promising for PBL sensing.

In the neutral atmosphere, the refractive index ($n$) is very close to unity, such that it is usually described in terms of refractivity defined as $N = (n - 1) \times 10^6$. The refractivity at GPS frequencies is related to the atmospheric pressure ($P$ in hPa), temperature ($T$ in Kelvin), and water vapor partial pressure ($P_w$ in hPa) through (Smith and Weintraub 1953)

$$N = b_1 \frac{P}{T} + b_2 \frac{P_w}{T^2}, \qquad (1)$$

where, $b_1$ = 77.6 K·hPa$^{-1}$ and $b_1$ = 3.73×10$^5$ K$^2$·hPa$^{-1}$. Consequently, based on the GPS retrieved refractivity, the atmospheric thermodynamic parameters such as density, temperature, pressure and humidity can be inferred (Kursinski et al. 1997; Rocken et al. 1997).

The refractivity is reported as a function of geometric height above mean-sea-level (MSL), whereas the bending angle is reported as a function of impact parameter, which is the product of refractive index and Earth's radius at the tangent point. The detailed description of GPS RO occultation technique can be found in earlier studies (e.g., Kursinski et al., 1997; Anthes et al., 2008).

In the geometric optics (GO) approximation to the propagation of electromagnetic radiation, the path of a ray passing through a region of varying refractive index is determined globally by Fermat's principle of least time and locally by Snell's law. Consider rays in a medium with spherical symmetry, i.e., where the refractive index only varies on

the radial direction, the bending angle ($\alpha$) can be described as the accumulated change in the ray path direction along a ray path such as:

$$\alpha(a) = -2a\int_a^\infty \frac{d\ln(n)}{dx}\frac{dx}{\sqrt{x^2-a^2}}\,. \tag{2}$$

The impact parameter, $a$, is a constant along one single ray path. It is also known as Bouguer's rule, which represents Snell's law in a spherically symmetric medium. Note that eqn (2) provides the forward calculation of bending angle $\alpha$ given a one-dimensional refractive index profile $n(r)$.

By inverting the equation through the Abelian transformation (or called Abel Inversion), the $n(r)$ can be expressed as a function of $\alpha$ and $a$ (Fjeldbo et al. 1971):

$$n(r) = \exp\left[\frac{1}{\pi}\int_a^\infty \frac{\alpha(x)dx}{\sqrt{x^2-a^2}}\right]. \tag{3}$$

Given impact parameter $a$ and the refractive index $n$, the radius $r$ at each tangent point can be derived according to Bouguer's formula:

$$r = \frac{a}{n(r)}\,. \tag{4}$$

In the regions where the water vapor is negligible, equation (1) reduces to $N=b_1 P/T$. As the saturation vapor pressure decreases rapidly with decreasing temperature according to Clausius-Clapeyron equation, the water vapor pressure $P_w$ can be neglected in the upper troposphere where temperature is low (e.g., $T$ < 250 K) (Kursinski et al., 2000; Hajj et al., 2002). Given the pressure (or dry pressure derived from hydrostatic balance) and RO refractivity (or density) profiles, accurate temperature profiles can be derived throughout the stratosphere down to mid-troposphere and below depending on latitudes, where the water vapor is negligible, e.g.,

$$T_{dry} = b_1\frac{P}{N} \tag{5}$$

Note that eqn (5) is generally called dry temperature, which will become colder than the real temperature in the presence of water vapor. Due to the presence of water vapor in the lower troposphere, the temperature and humidity can't be directly retrieved solely from RO refractivity. The external a-priori information of either temperature or humidity becomes necessary. Generally the water vapor uncertainty far exceeds the pressure and temperature uncertainties due to its large variation. Given the precise measurement of RO refractivity and the independent knowledge of temperature (e.g., from in-situ observations, global model analysis, reanalysis or climatology), the water vapor pressure can be derived. It is also possible to obtain optimal estimation of the water vapor, temperature and pressure through the variational methods. These methods combine the occultation measurements (e.g., refractivity) with the a-priori (or background) atmospheric information in a statistically optimal way (e.g., Zou et al., 1995; Healy and Eyre, 2000).

Even though RO water vapor retrieval or temperature retrieval are generally easy to be used, such retrieval can no longer be treated as independent RO observables as they will embrace errors from the a-priori information used. On the other hand, the other three RO observables (e.g., bending angle, refractivity and dry temperature) can be treated as model-independent GPS RO observables.

## 2.2 ECMWF reanalysis

We examine the ECMWF global reanalysis (ERA-interim, ERA-i), which has 1 ☒1 ☐ longitude-latitude horizontal grid, 60 vertical layers with the top of the atmosphere located at 0.1 hPa. The six-hourly reanalysis outputs (00UT, 06UT, 12UT and 18UT) have about 21 levels from surface to ~5 km, starting with a resolution of about 25 m near the ground, decreasing to about 200 m around 1 km altitude (von Engeln and Teixeira, 2013). This study will focus on year-2008 data over global oceans. The vertical profiles of all conventional parameters and GPSRO parameters (listed in Table 1) will be directly extracted or derived from the reanalysis at each grid.

### 2.2.1 Simulated GPS RO observables from ERA-i

Given the ERA-i pressure, temperature and specific humidity profiles at each grid, GPS RO refractivity can be easily calculated based on eqn (1). The dry temperature ($T_{dry}$) can also be derived based on eqn (5). Note that the dry temperature is the same as the real temperature in the dry atmosphere (e.g., stratosphere and upper troposphere), but become colder than the real temperature in the lower troposphere especially inside the PBL where moisture could contribute to the refractivity significantly. The dry temperature is a function of both temperature and humidity and therefore could be a unique and powerful parameter to sense the PBLH where vertical variations of thermal or moisture gradients are located.

It is worth noting that the vertical profiles of pressure, temperature, specific humidity and relative humidity in ERA-i are given as a function of geopotential heights at each grid, whereas the GPS RO observables are reference to the geometric height above mean sea level. The difference between the geometric height and the geopotential height inside the PBL (generally below 5 km) are small. Therefore, we simply use the geopotential height in the simulated GPS RO observables.

Assuming a spherically symmetrical atmosphere, one can further compute the bending angle profile as would be observed by GPS RO given a refractivity profile. With the spherically symmetric atmosphere assumption, the integration of refractivity along the ray path can be simplified when integrating as a function of impact parameter based on the Bouguer's rule. For example, equation (2) provides the forward calculation of bending angle $\alpha$ given the refractive index profile $n(r)$. In general, the impact parameter is a monotonic function of height. Therefore, the standard integration technique (e.g., Simpson's rule) can be directly applied to solve for the bending. Though, the singularity at the lower and upper boundary (e.g., $x=a$ and $x=\infty$, respectively) needs to be resolved. For example, it is practical to use 100 km as the upper boundary layer instead of infinity or the

satellite altitude. However, a more elegant way mathematically is to revise the integration through proper function substitution, which removes the singularity in the integration and improves accuracy of the integration (e.g., Hajj et al., 2002, Xie, 2006; Xie et al., 2006).

In the moist lower troposphere, especially over subtropical eastern oceans, a very sharp temperature inversion and a large negative moisture gradient are often observed at the top of the PBL (von Engeln and Teixeira, 2004; Xie et al., 2012). These sharp temperature and moisture gradients give rise to a large negative refractivity gradient that causes a large bending of GPS RO signal paths. The so-called ducting condition (also referred to as super-refraction) occurs when the vertical refractivity gradient exceeds a critical value, i.e., $dN/dz < -1/r_e \approx -157$ $N$-unit km$^{-1}$ ($r_e$ is the curvature radius of the Earth). At the upper and lower edges of the ducting layer, the refractivity gradient equals the critical value (i.e., critical refraction).

In the presence of ducting, the impact parameter is no longer a monotonic function of height (Sokolovskiy, 2003; Ao et al., 2003; Xie et al., 2006). The forward bending calculation in eqn (2) will need to remove the vertical interval where a non-monotonic relation between the impact parameter and height exists inside the ducting layer and an adjacent layer right below. Moreover, the bending angle will become infinite at the upper edge of the ducting layer where the critical refraction occurs. The singularity of the integration due to the critical refraction will require special mathematical treatment as discussed in Xie et al. (2006).

The refractivity is a function of pressure, temperature and water vapor pressure according to eqn (1). The negative refractivity gradient can have contributions from all these three factors, such as

$$\delta N = b_1 \frac{\delta P}{T} - \left( b_1 P + 2 b_2 \frac{P_w}{T} \right) \frac{\delta T}{T^2} + b_2 \frac{\delta P_w}{T^2} \ . \qquad (6)$$

Replacing $P_w$ by the specific humidity, $q$, according to $q = \varepsilon \cdot P_w / P$ ($\varepsilon = 0.622$), we have

$$\delta N = c_1 \delta P - c_2 \delta T + c_3 \delta q \ , \qquad (7)$$

where,

$$c_1 = \left( b_1 + \frac{b_2 q}{\varepsilon T} \right) / T, \qquad c_2 = \left( b_1 P + 2 b_2 \frac{P \cdot q}{\varepsilon T} \right) / T^2, \qquad c_3 = \frac{b_2 P}{\varepsilon T^2} \ . \qquad (8)$$

It is important to note that the opposite changes in temperature increase and moisture drop across the PBL top lead to an enhanced decrease in refractivity, which will lead to a decrease in bending angle.

Similarly, the vertical gradient of dry temperature can be expressed as a function of temperature, humidity and pressure gradients according to eqns (5) and (7), such as:

$$\delta T_{dry} = d_1 \delta P + d_2 \delta T - d_3 \delta q, \qquad (9)$$

where,

$$d_1 = b_1 (N - c_1 P)/N^2, \; d_2 = b_1 c_2 P / N^2 \text{ and } d_3 = b_1 c_3 P / N^2 \qquad (10)$$

Therefore the vertical gradient of dry temperature preserves the behaviour of refractivity gradient and will capture both the temperature inversion and negative water vapour gradients.

## 2.3 PBL height definitions

As discussed in Section 1, numerous definitions of PBL heights have been proposed based on various physical parameters. Conventional PBLH definitions are generally based on the vertical profile of atmospheric thermodynamic parameters, such as temperature, humidity and their derivable (e.g., Seidal et al., 2010). The PBLH is most commonly defined as the altitude where the vertical change of the selected parameter become a maximum, which generally corresponds to the altitude of maximum (positive) or minimum (negative) gradient.

For example, the PBL height often refers to the temperature inversion base, where the temperature increases at higher altitude instead of the normal decreasing with height. The inversion layer marks a stable layer that often results in a decrease in moisture across the inversion layer. Similar to relative humidity, the RO observables, such as refractivity, bending and dry temperature, are functions of both temperature and specific humidity. The advantage of such parameters is that they capture both the positive temperature and negative moisture gradients, without cancelling out each other. This could make them more attractive as compared with the conventional temperature or humidity only PBL height definitions. For example the temperature-based PBLH definition could become problematic in the presence of a weak inversion but with some moisture gradient, whereas, the humidity-based PBLH definitions (e.g., $q$) will have problems over dry region with only temperature inversion at PBL top. In such case, the RO refractivity and dry temperature based PBLH definitions could potentially be more general applicable.

In this study, we use the simple gradient method to define the PBL height. At each reanalysis grid-point, vertical profiles of various parameters (Table 1) were extracted or derived. Note that the ERA-interim has un-even vertical grids, with much denser grids near the surface and increasing sampling interval at higher altitudes. The gradient calculation can be sensitive to the vertical sampling of the data (e.g., Seidel et al., 2010). To ensure consistent PBL height quality derived with the gradient method, all ECMWF vertical profiles are interpolated on a 10 m vertical grid from surface up to 5 km. The vertical gradients are further computed for each parameter. The altitude with the maximum/minimum gradient for each parameter is then defined as the PBL height. For example, the PBLHs correspond to altitudes of the maximum (positive) gradients for temperature and dry temperature, but the minimum (negative) gradients for specific/relative humidity, refractivity and bending angle (i.e., Table 1).

In this project, we mainly focus on the elevated PBL height. In order to exclude the surface based inversion that is often seen over tropical and subtropical oceans (von Englen and Teixeira, 2004), we exclude data points below 300m in our analysis.

# 3. PBL Height Climatology

## 3.1 Seasonal-mean Global PBL Height Climatology

Previous study demonstrated the relative humidity (*RH*) based PBLH method appears to capture well the inversion that caps the convective boundary layer due to its temperature and humidity dependence (von Engeln and Teixeira, 2013). The *RH* based PBL height climatology at four seasons (DJF, MAM, JJA and SON) is derived from one-year (2008) ERA-i reanalysis as shown in Fig. 1.1, respectively. The seasonal climatology is consistent with previous study by von Engeln and Teixeira (2013). The most dominant features are the dipole structure over the subtropical eastern oceans, with a persistent shallow PBL (~1 km) centered near the west coasts of the continents, and a much deeper PBL (~2 km) westward centered at the trade-wind region (e.g., near Hawaii in NE Pacific). These features are clearly seen in both northern and southern Pacific and Atlantic Oceans as well as Southern Indian Ocean in all seasons. The cool sea surface temperature (caused by deep ocean upwelling) together with the strong subsidence in the free troposphere (due to the descending blanch of Hadley cell) results in a very shallow and stable PBL inversion layer over the region. The PBL deepens westward with the increasing SST and weaker subsidence, and reaches over ~2 km in the trade-wind area. Shallow PBL is also often seen over polar latitudes. The deepest PBL are seen in the tropical ITCZ, especially over the Pacific where deep convection dominates the region. Relative deep PBL are also seen over the western Pacific in boreal winter (DJF) and spring (MAM) seasons. Interestingly, rather shallow PBL are seen over the western Pacific warm pool regions all year round.

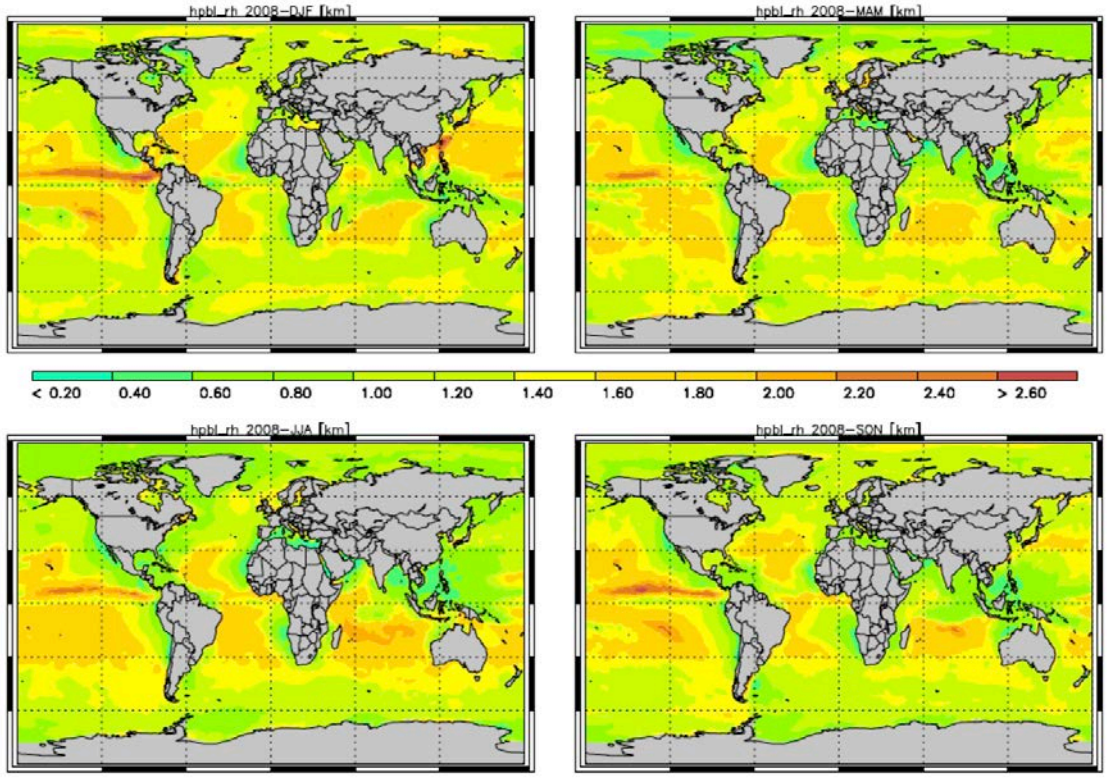


Figure 1.1 Seasonal-mean *RH* based PBLH climatology at four seasons (DJF, MAM, JJA and SON) in 2008.

Similarly, the seasonal-mean PBLH climatology based on the other physical parameters (refractivity $PBLH_N$, specific humidity $PBLH_q$, temperature $PBLH_T$, and dry temperature $PBLH_{Tdry}$) can also be derived with the gradient method. For better comparison, the PBLH climatology of the four parameters is displayed together at each season (e.g., DJF, MAM, JJA, SON) in Fig. 1.2-1.5, respectively. Overall, all PBLH climatology reveals similar spatial pattern, such as the dipole structure over subtropics eastern oceans as seen in $PBLH_{RH}$. However, significant difference can be seen among different definitions. The $PBLH_N$ shows most consistent pattern with the specific humidity except polar region. Note however, in the boreal summer over Arctic, the two share much more similarity. In the other seasons (DJF, MAM and SON), however, the $PBLH_q$ becomes systematically higher than $PBLH_N$. Both $PBLH_N$ and $PBLH_q$ are significantly lower than the other PBLH definitions from tropics to mid-latitude. On the other hand, $PBLH_T$ is rather consistent with the $PBLH_{RH}$ globally with most significant difference in tropics near the ITCZ. Both the $PBLH_{Tdry}$ and $PBLH_T$ show very consistent pattern with $PBLH_{RH}$ at all seasons except the polar region.

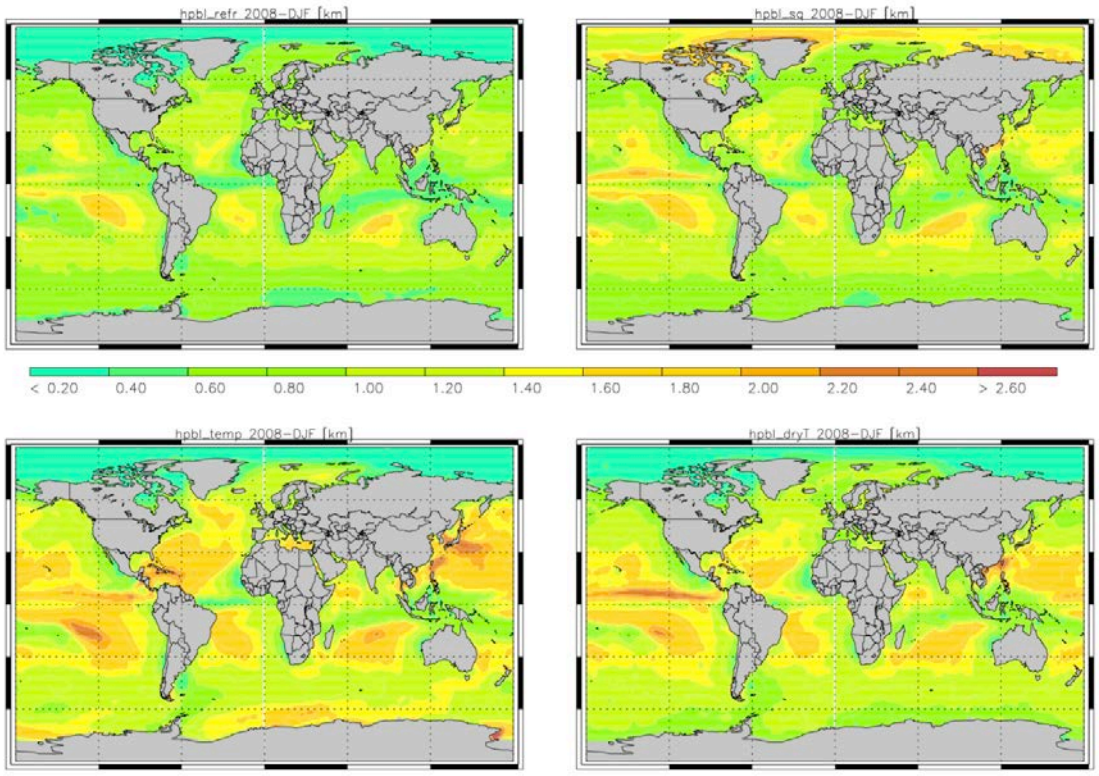


Figure 1.2 Seasonal mean PBL height climatology in boreal winter season (2008-DJF) based on refractivity, specific humidity, temperature and dry temperature, respectively.

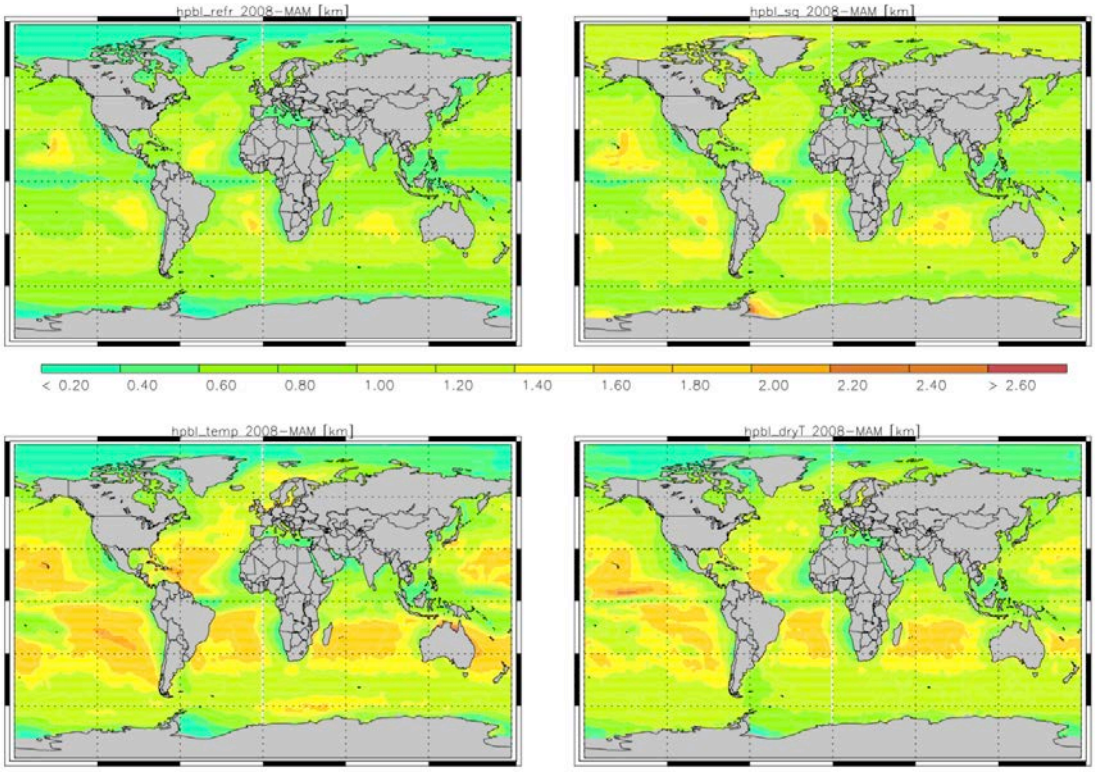


Figure 1.3 Same as Fig. 1.2 but in the boreal spring season (2008-MAM).

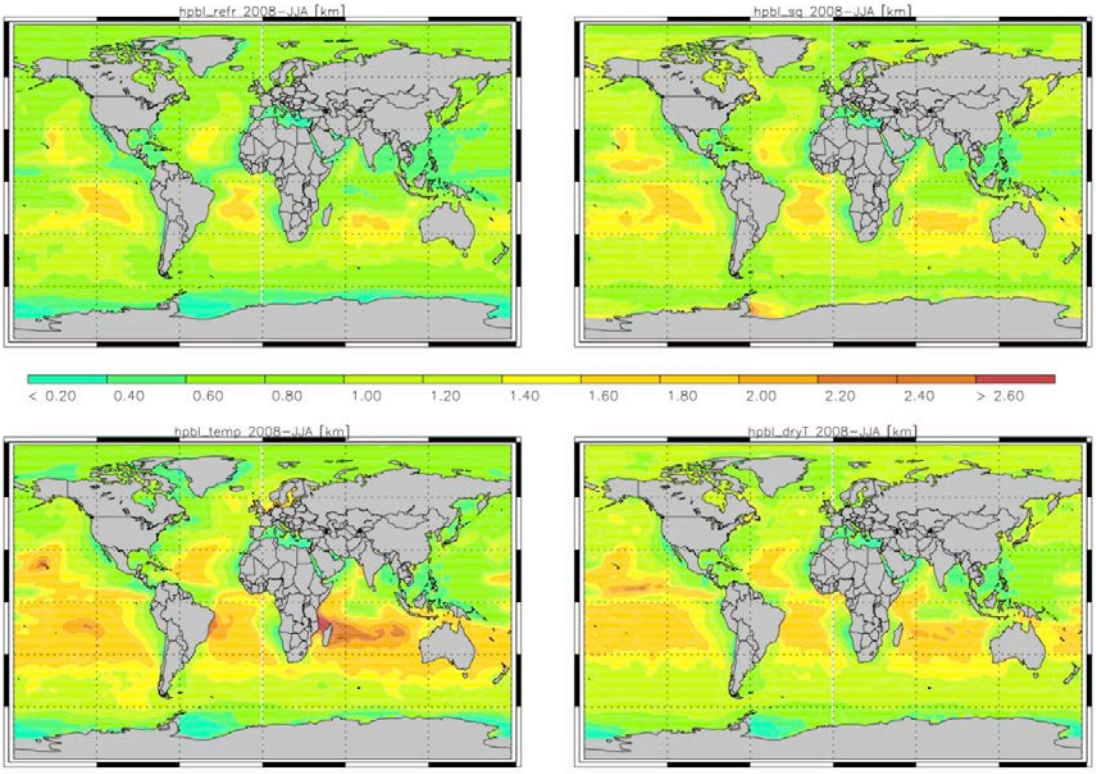


Figure 1.4 Same as Fig. 1.2 but in the boreal summer season (2008-JJA).

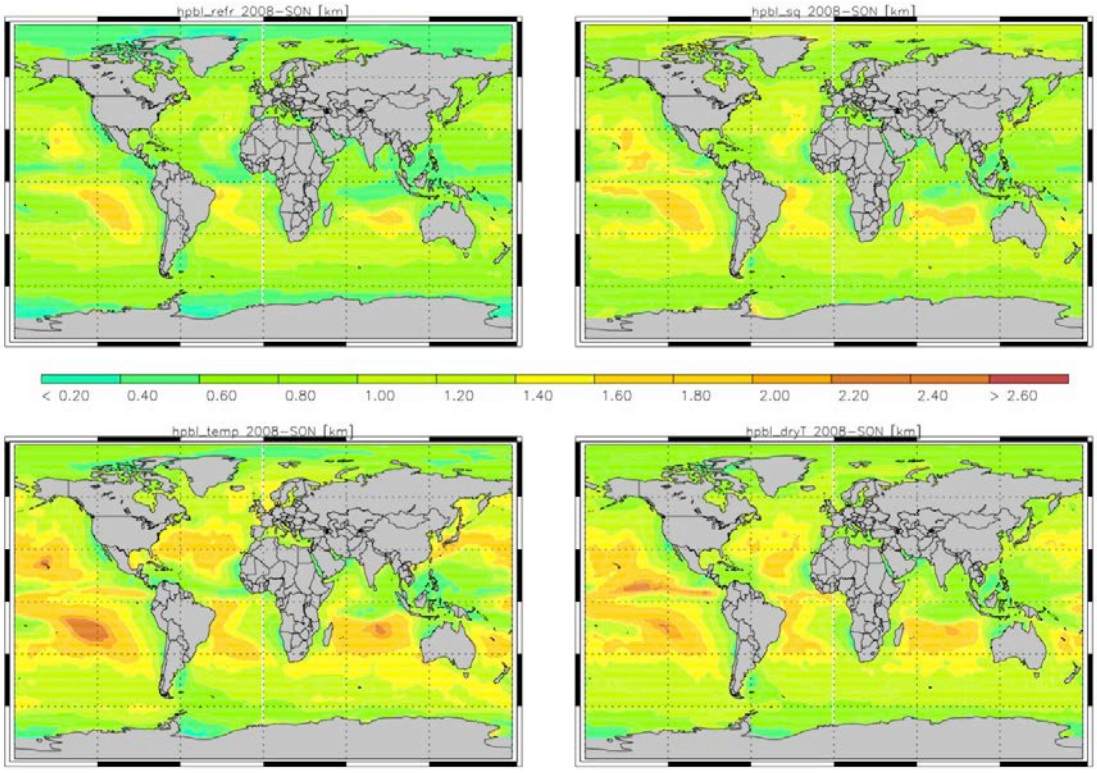


Figure 1.5 Same as Fig. 1.2 but in the boreal autumn season (2008-SON).

## 3.2 PBL height difference from *RH* based definition

In the previous section, systematic differences among various PBLH definitions are clearly seen in Figs.1.1-1.5. In this section, we compute the difference between each PBLH definition as reference to the relative humidity based PBLH ($PBLH_{RH}$) for each season.

Figure 2.1 shows the four-panel plots of PBLH difference of refractivity, specific humidity, temperature and dry temperature as compared to $PBLH_{RH}$ in boreal winter season, respectively. The PBLH differences in the other three seasons are displayed in Fig. 2.2-2.4, respectively. In all seasons, the $PBLH_N$ and $PBLH_q$ show largest discrepancy from the $PBLH_{RH}$. Systematic negative biases are clearly seen in $PBLH_N$ globally with a maximum of about −2 km over ITCZ in tropical Pacific, Atlantic and Indian Oceans. There is also about −1 km bias from low to high latitudes except the subtropical eastern oceans near the coast of major continents. The biases also show rather large seasonal variation especially over both north and south polar latitudes.

$PBLH_q$ shows very similar seasonal climatology as $PBLH_N$. Not surprisingly, the spatial pattern of low bias in $PBLH_q$ as compared with $PBLH_{RH}$ is very similar to the bias of $PBLH_N$ except the polar latitudes. Over Arctic Ocean, $PBLH_q$ is systematically higher (positive bias) than $PBLH_{RH}$.

On the other hand, the $PBLH_T$ shows rather consistent spatial pattern as compared with $PBLH_{RH}$, which leads to a smaller bias (within 200 m) overall globally except some negative bias concentrated over tropics and high latitudes (especially dry winter season).

Interestingly, the $PBLH_{Tdry}$ shows remarkable consistence with the $PBLH_{RH}$ over much of the globe from tropics to the mid-latitude except some low (negative) biases over polar region especially over winter Arctic Ocean. Such low biases are also clearly seen in the $PBLH_T$ with similar spatial pattern and amplitude, which confirms the similarity between $PBLH_T$ and $PBLH_{Tdry}$ over polar region.

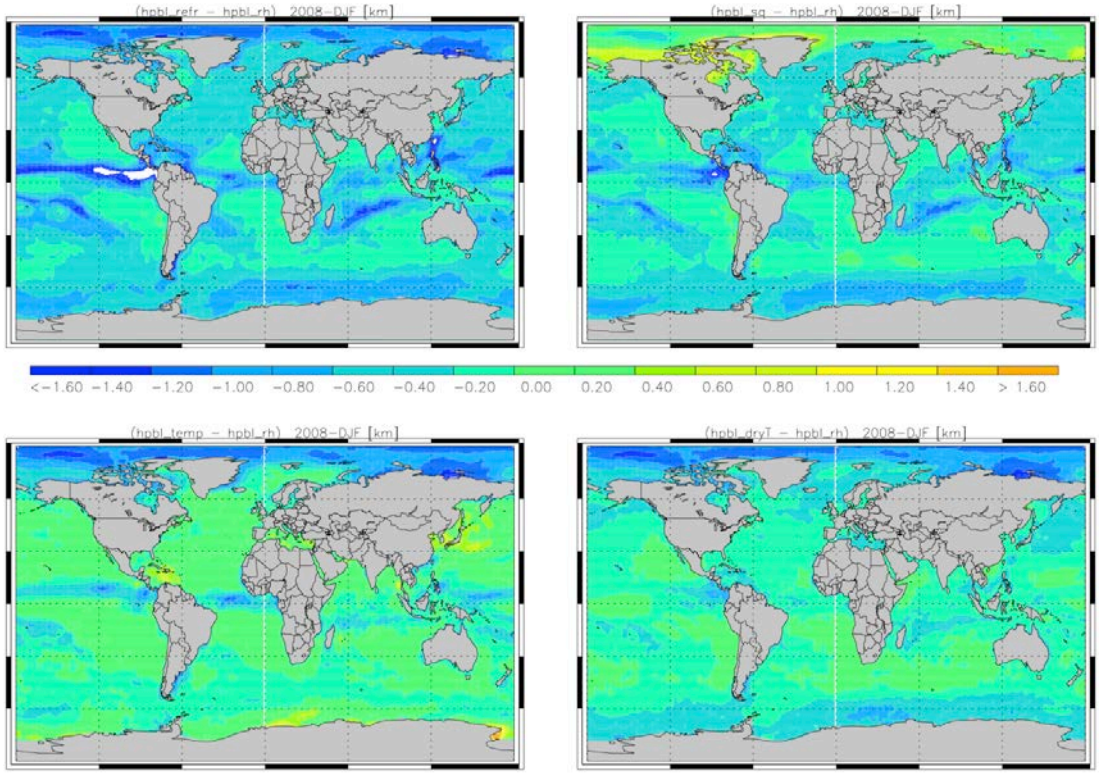


Figure 2.1 Difference of seasonal mean PBLH climatology ($PBLH_N$, $PBLH_q$, $PBLH_T$, and $PBLH_{Tdry}$) from $PBLH_{RH}$ in boreal winter (2008-DJF). Note the white color represents the region with PBLH more than 1.6 km below $PBLH_{RH}$.

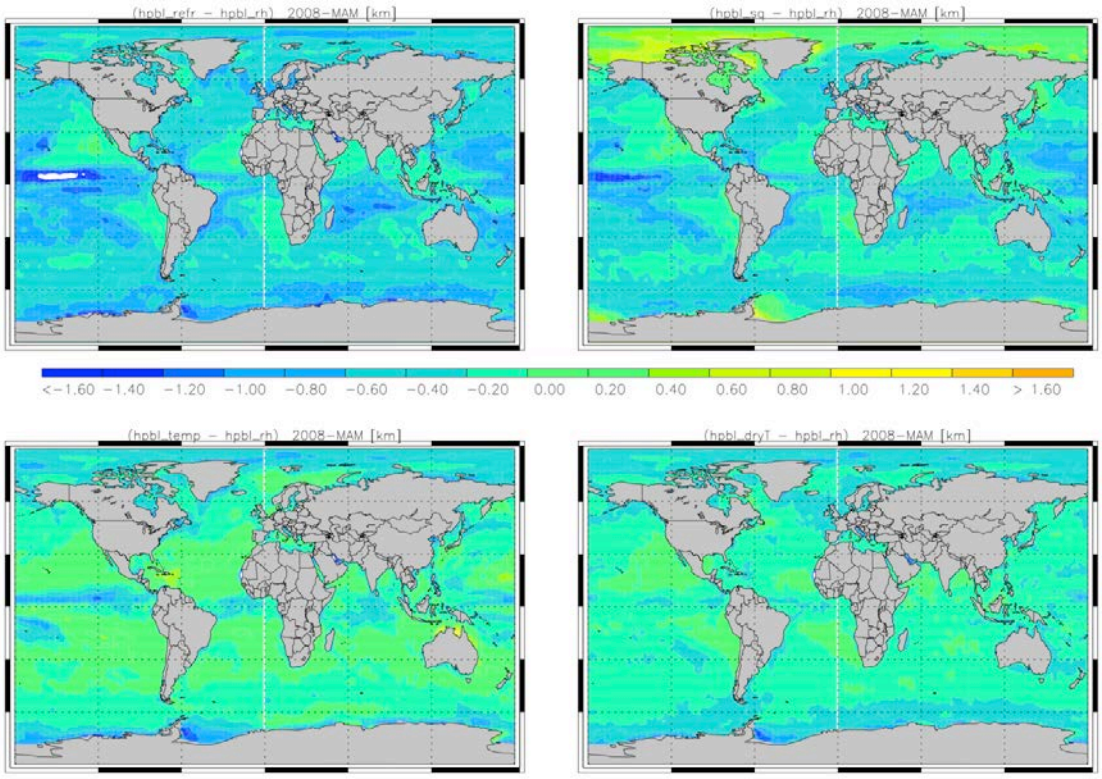


Figure 2.2 Same as Fig. 2.1 but in boreal spring season (2008-MAM).

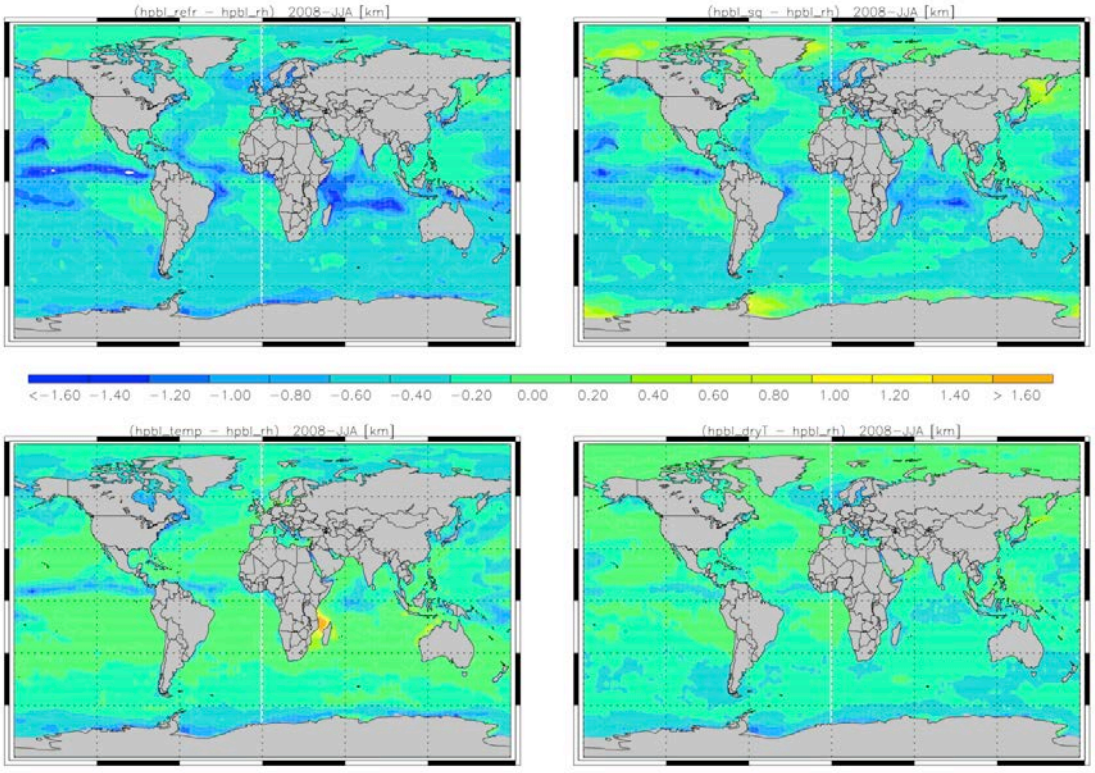


Figure 2.3 Same as Fig. 2.1 but in boreal summer season (2008-JJA).

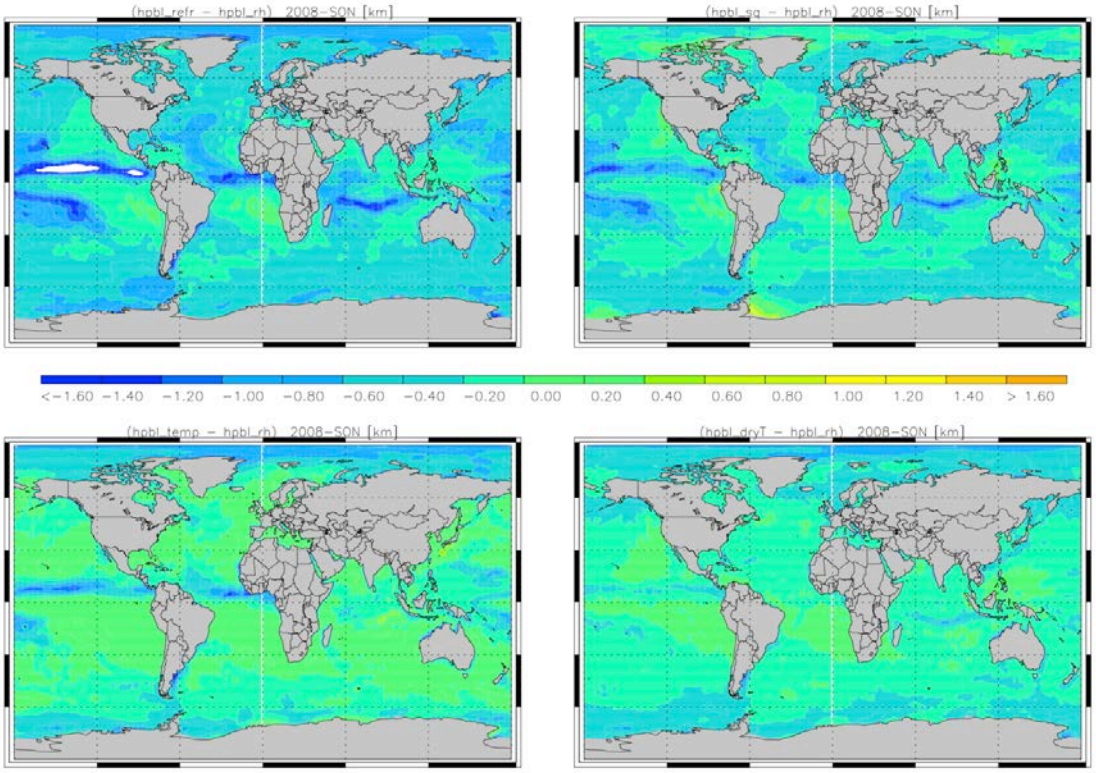


Figure 2.4 Same as Fig. 2.1 but in boreal autumn season (2008-SON).

## 3.3 PBL Transect from stratus to trade cumulus

In recent years, significant research effort has been focusing on the transect over eastern Pacific that was introduced by the GCSS (GEWEX Cloud System Studies) Pacific Cross-section Intercomparison (GPCI) (Teixeira et al. 2011). The transect extends from the stratocumulus regions off the coast of California, across the shallow convection dominated trade winds (near Hawaii), to the deep convection regions of the ITCZ near equator (i.e., from 35°N, 125°W to 1°S, 173°W). Similarly, the transect at the southeast Pacific Ocean around 20°S from near coast of the South America extending westward to the open ocean also attract many research campaigns to study the cloud transition from stratus to trade cumulus (e.g., Bretherton et al., 2010, Wood et al., 2011). Both transects are regions critical for understanding the tropical and subtropical cloud processes and their transition, which remain big uncertainty in weather and climate prediction models.

Figure 3.1 shows the seasonal mean PBLHs as a function of latitude (every 3 degree) along the GPCI transect extending from the western coast of the south California heading southwest to the equator. All five parameters lead to very consistent PBLHs from 35°N (off coast of south California) to ~20°N (near Hawaii) with small variation as shown in the standard deviation of $PBLH_{RH}$. However, significant differences among PBLH definitions are observed further south of ~20°N, where much larger PBLH variation are also seen. Specifically, the $PBLH_N$ and $PBLH_q$ are systematically lower than the other three definitions. The $PBLH_{RH}$ and $PBLH_{Tdry}$ are most consistent with each other along the

whole transect. It is also worth noting that seasonal variation of the PBLHs are observed, for example, the summer season (JJA) shows the least PBLH difference and variations from 35°S all the way to around 14°S as compared to the other seasons.

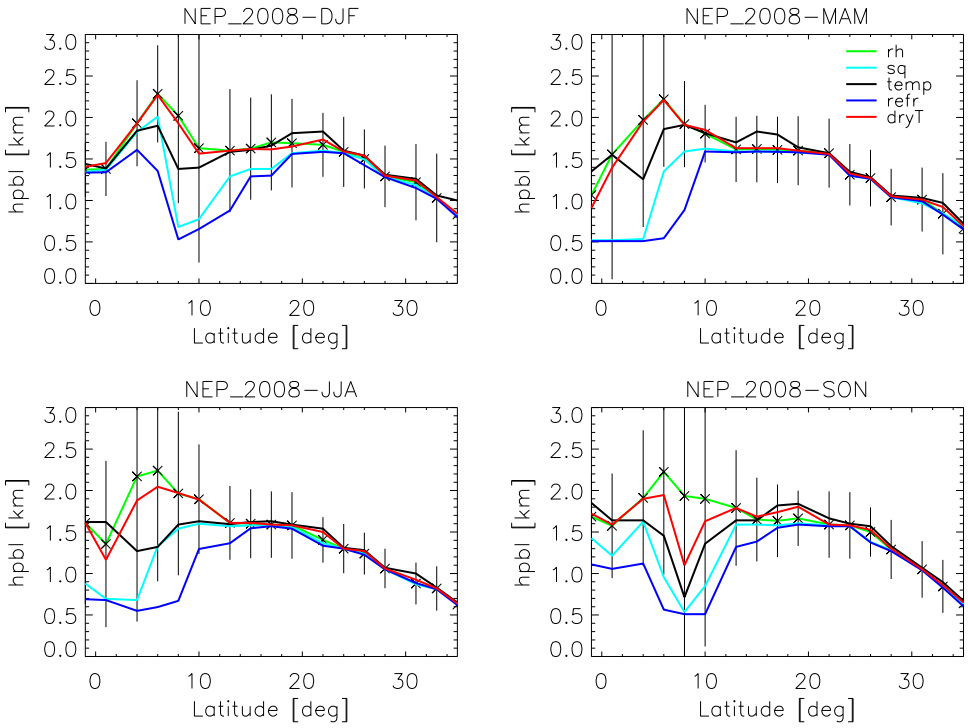


Figure 3.1 Four seasonal mean PBLHs along the GPCI transect from off coast of southern California heading southwest to the equator (i.e., from [35°N, 125°W] to [1°S, 173°W]). The error bar shows the standard deviation of $PBLH_{RH}$ variations.

Similarly, Figure 3.2 shows the seasonal mean PBLHs along 20°S transect extending from the western coast of the South America (~70°W, near Peru and Chile) heading westward to the open ocean at ~150°W. Similar to the GPCI transect, PBLHs shows the minimum difference from 70°W (off coast of Peru) to ~110°W with small variation as shown in the standard deviation of $PBLH_{RH}$. However, significant differences among PBLH definitions are observed further west of ~110°W, where much larger PBLH variations are observed. Again, the $PBLH_{RH}$ and $PBLH_{Tdry}$ are most consistent with each other throughout the transect. The $PBLH_N$ and $PBLH_q$ show systematically lower values when compared to other three definitions. Moreover, PBLHs (westward of 110°W) show the maximum and minimum variation in MAM season and JJA season, respectively,.

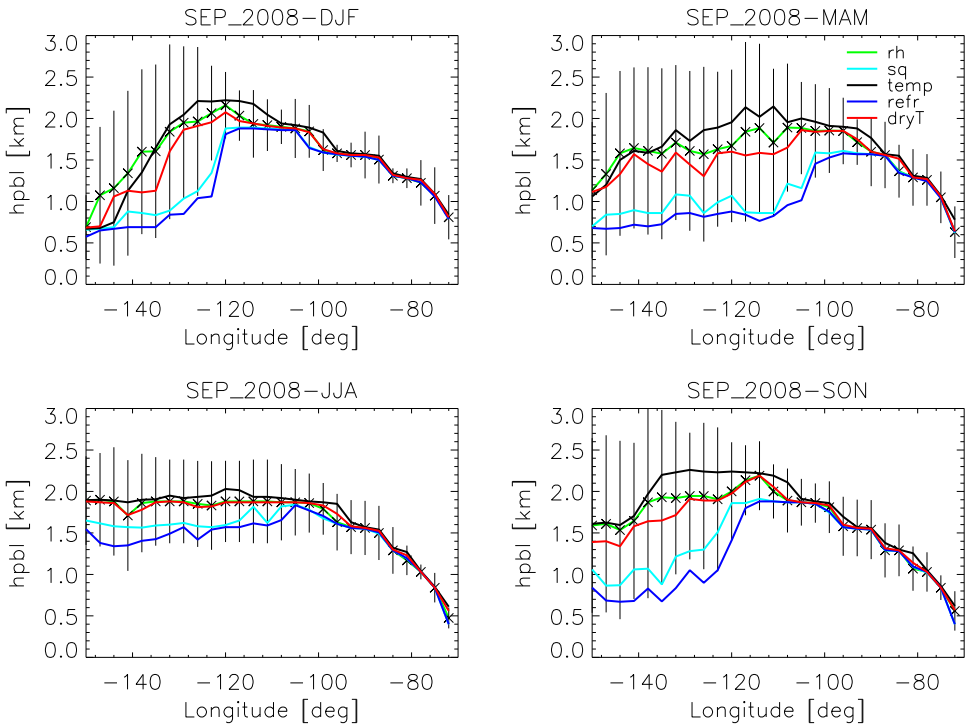


Figure 3.2 Four seasonal mean PBLHs along 20°S transect from off coast of South America westward to 150°W over Southeastern Pacific Ocean. The error bars represent the standard deviation of $PBLH_{RH}$.

## 3.4 Monthly mean PBL height correlation

Based on the monthly mean PBLH climatology (not shown), we further investigate the correlation between individual PBLH definitions. The linear Pearson correlation coefficient between $PBLH_{RH}$ and $PBLH_N$ is shown in Fig. 4.1. Pearson's linear correlation coefficient can range from −1 to 1 (−100%–100%). As indicated in the four monthly plots (January, April, July and October), high correlation is only found over subtropical eastern oceans near the west coast of the major continents, where sharp inversion and moisture gradient prevails across the stratus-topped PBL (e.g., west coast of Northern & Southern America and Africa, India and Australia). Significant decrease in correlation is seen near the trade wind region (e.g., near Hawaii in NE Pacific). Tropics and high latitudes show no significant correlation, which is consistent with the significant difference between the two definitions in Figs. 2.1-2.4. Very low or almost no correlations are seen over the polar regions.

The $PBLH_q$ shows a general higher correlation with $PBLH_{RH}$ overall (Fig. 4.2) as compared with $PBLH_N$ (Fig. 4.1) but exhibits very similar spatial pattern. For example the highest correlation is also only seen over subtropical eastern oceans and much lower correlations over trade wind, middle and high latitudes. The similarity between $PBLH_q$ and $PBLH_N$ is apparent in the seasonal climatology (Figs. 1.2-1.5) and is further confirmed in Fig. 4.5, which shows very high correlation (>60%) across most of the subtropical oceans,

including the near shore and off shore trade-wind regions. But tropics and polar region show rather low correlations.

Again, the $PBLH_T$ (Fig. 4.3) shows very similar correlation spatial pattern as $PBLH_q$ and $PBLH_N$ with only high correlation over subtropical eastern oceans near the continent and rather low correlation elsewhere. Especially low correlation is found over tropics and polar region.

Interestingly, $PBLH_{Tdry}$ shows the highest correlation with $PBLH_{RH}$ as compared to other definitions. High correlation is shown from tropic to the mid-latitude rather homogeneously in all four seasons. While low correlation is generally seen over polar region especially during the polar winter. A slight increase in correlation over the Arctic Ocean is obvious during the boreal summer months (e.g., July).

Overall, the $PBLH_{RH}$ shows very high correlations (>70%) with all the other PBLH definitions over subtropical eastern oceans near the west coast of major continents. However, generally lower correlations are seen over tropics and high-latitude as well as trade-wind regions as seen in $PBLH_N$, $PBLH_q$ and $PBLH_T$. On the other hand, the $PBLH_{Tdry}$ shows highest correlation with $PBLH_{RH}$ globally except polar region especially in winter months. Note the polar region is dominated by the shallow PBL with either surface based inversion (only a couple hundred meters) or shallow elevated inversion (up to several hundred meters) (e.g., Tjernström and Graversen, 2009). The very dry condition could potentially make the humidity based PBLH definition not reliable, especially the specific humidity. The larger standard deviation of $PBLH_q$ over high-latitude (not shown), as compared with $PBLH_T$ and $PBLH_{Tdry}$ indicates the $PBLH_q$ becomes problematic in very dry condition.

The relative humidity depends on both absolute humidity and also the temperature through the saturation pressure. However, during the polar winter, the surface air temperature is generally below 250 K, when the saturated vapor pressure becomes very low (i.e., less than 1 hPa). The relative humidity becomes highly sensitive to the variation of the absolute water vapor pressure, which could lead to larger uncertainty in identifying the PBLH as compared with the temperature based PBLH definition. On the other hand, the $PBLH_{Tdry}$ is much more consistent with $PBLH_T$ (Fig. 1.2-1.5) over polar region, which is further confirmed by the high correlation in Fig. 4.8 (January). This indicates that dry temperature potentially has the advantage of capturing the temperature inversion better than the relative humidity in very dry condition.

It is interesting to note that both the RO observables: refractivity ($N$) and dry temperature ($Tdry$) are temperature, humidity and pressure dependent. Therefore their gradient will be closely related to the gradients of temperature, humidity and pressure. In general, at the PBL height (e.g., below 5 km), the temperature, and especially the humidity gradient, will dominate the gradient in refractivity and dry temperature, whereas the pressure gradient only has minimum contribution. Note, however, that the refractivity gradient is generally dominated by the moisture gradient but not the temperature inversion (Ao, 2007). The dry temperature gradient has similar behavior but could be more sensitive to the temperature gradient when moisture decreases. The high sensitivity of $T_{dry}$ to the humidity is well demonstrated by the very high correlation between $PBLH_{Tdry}$ and $PBLH_q$ in subtropics and

mid-latitude (Fig. 4.9, whereas very low or no correlation between the two are seen over the extremely dry polar winter, e.g., Arctic in January and Antarctic in July). On the other hand, high correlation between the $PBLH_{Tdry}$ and $PBLH_T$ over polar winter (Fig. 4.8) clearly demonstrates the absence of moisture when $T_{dry}$ becomes close to absolute air temperature. On the contrary, no correlation is found between $PBLH_q$ and $PBLH_T$ (Fig. 4.10) indicating the problem of using the specific humidity to define the PBLH over high-latitude dry regions.

Overall the $PBLH_{Tdry}$ is highly correlated with $PBLH_{RH}$ from tropics to the mid-latitude, and is also highly correlated with $PBLH_T$ over high latitude, especially over polar winter. This implies that the dry temperature presents high sensitivity to both temperature and humidity gradients and could be widely applied globally for various type of PBL ranging from moist PBL in the low latitude to the dry PBL over high latitudes.

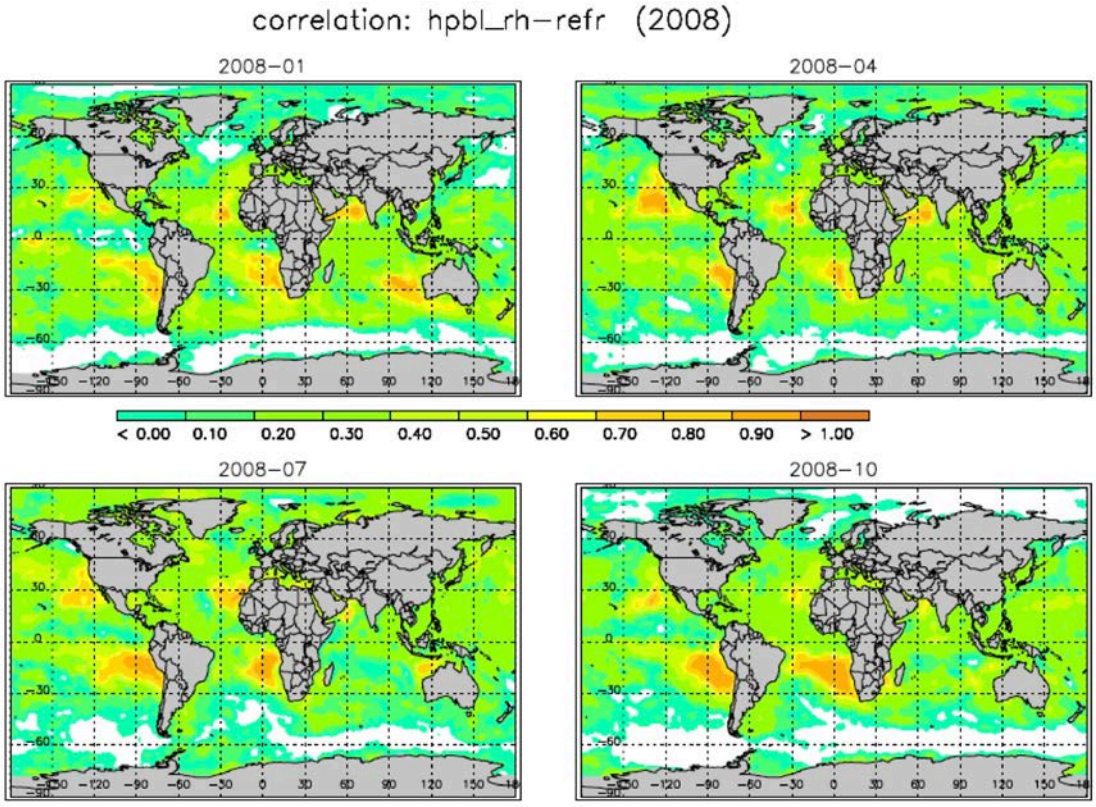


Figure 4.1 Monthly correlation coefficient between $PBLH_{RH}$ and $PBLH_N$ in January, April, July and October 2008, respectively. Note the white areas refer to very weak correlation with the correlation coefficient slightly less than zero.

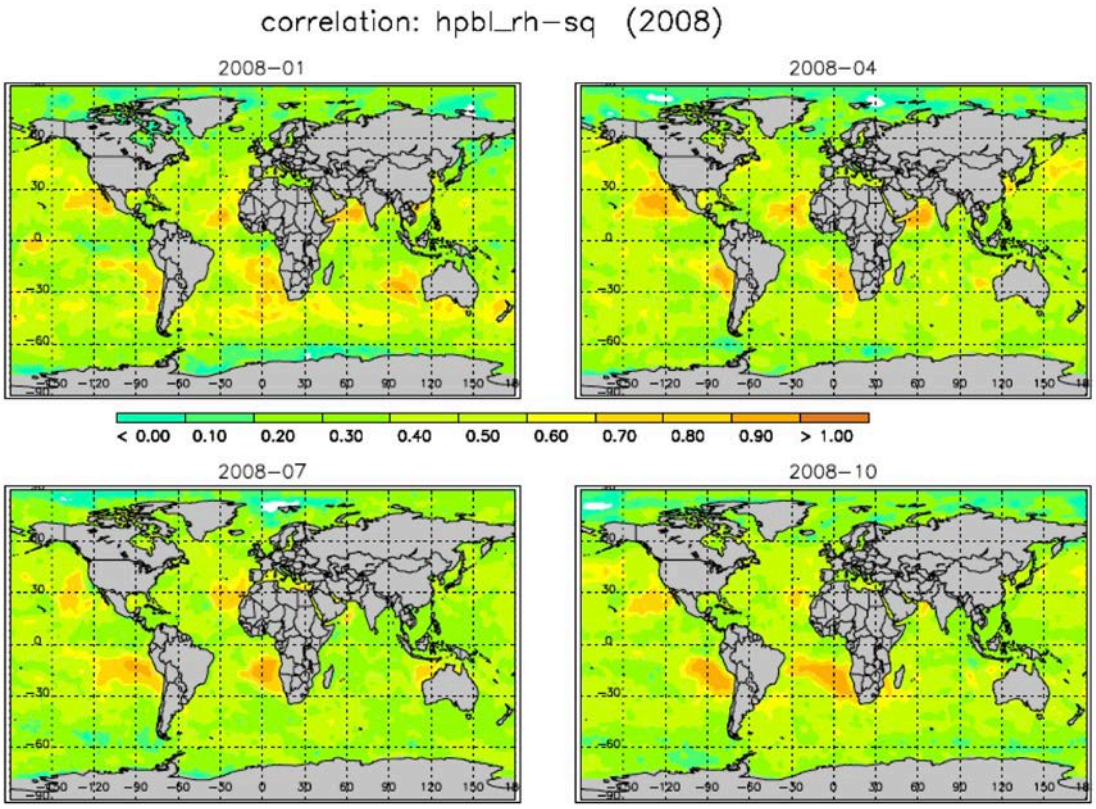


Figure 4.2 Same as Fig. 4.1 but the correlation coefficient between $PBLH_{RH}$ and $PBLH_q$.

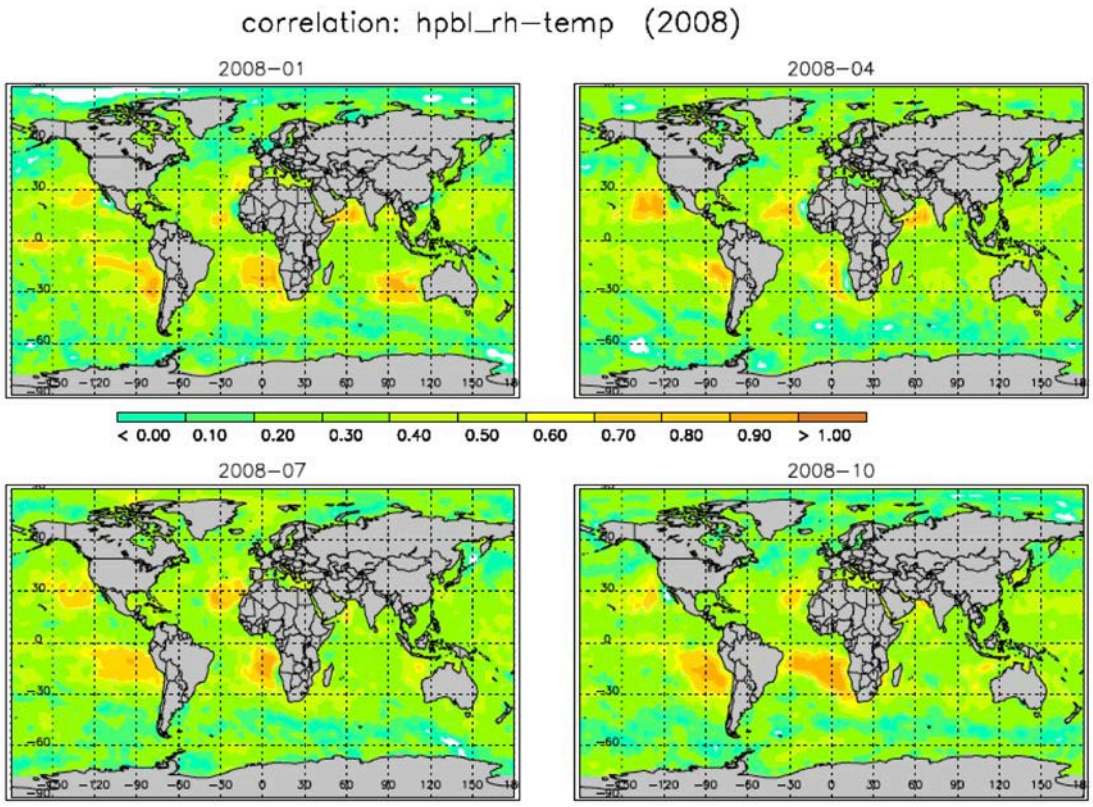


Figure 4.3 Same as Fig. 4.1 but the correlation coefficient between $PBLH_{RH}$ and $PBLH_T$.

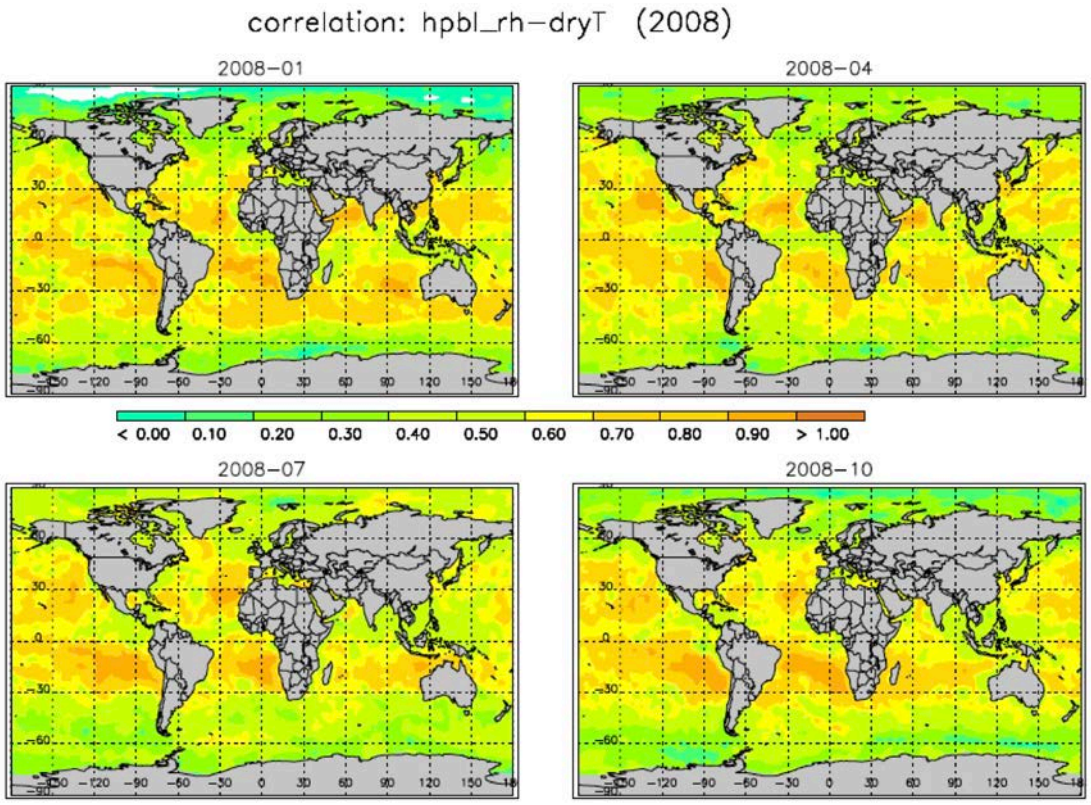


Figure 4.4 Same as Fig. 4.1 but the correlation coefficient between $PBLH_{RH}$ and $PBLH_{Tdry}$.

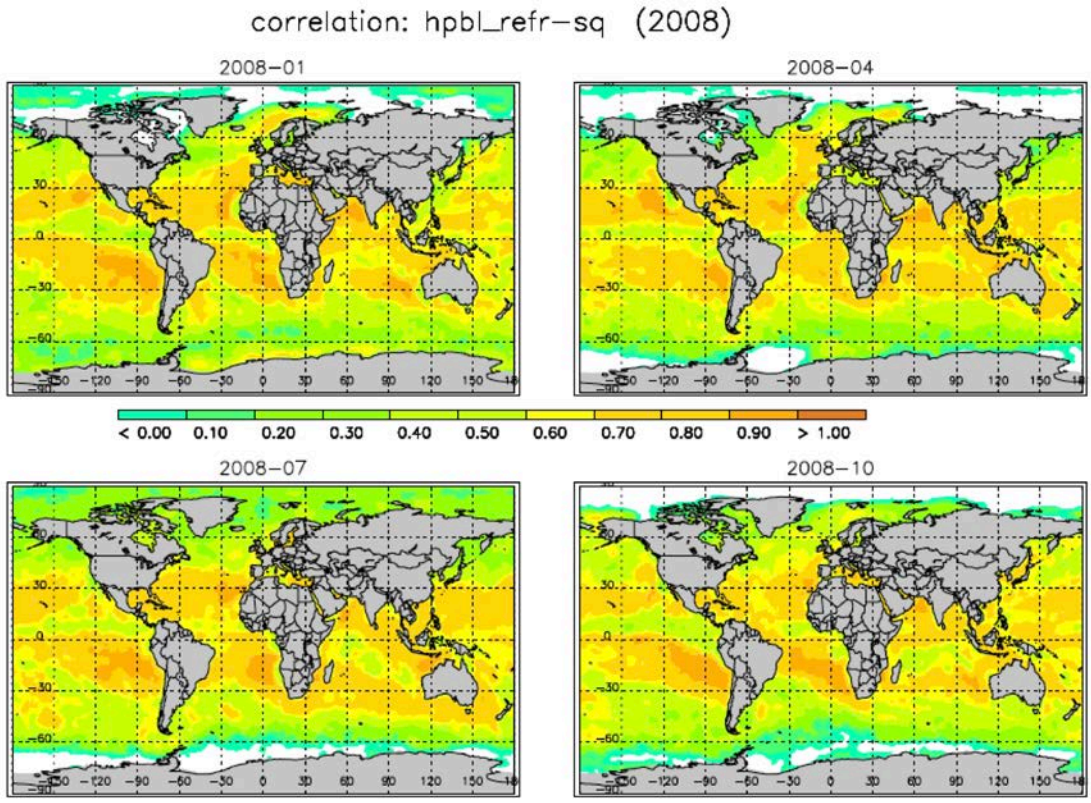


Figure 4.5 Same as Fig. 4.1 but the correlation coefficient between $PBLH_N$ and $PBLH_q$.

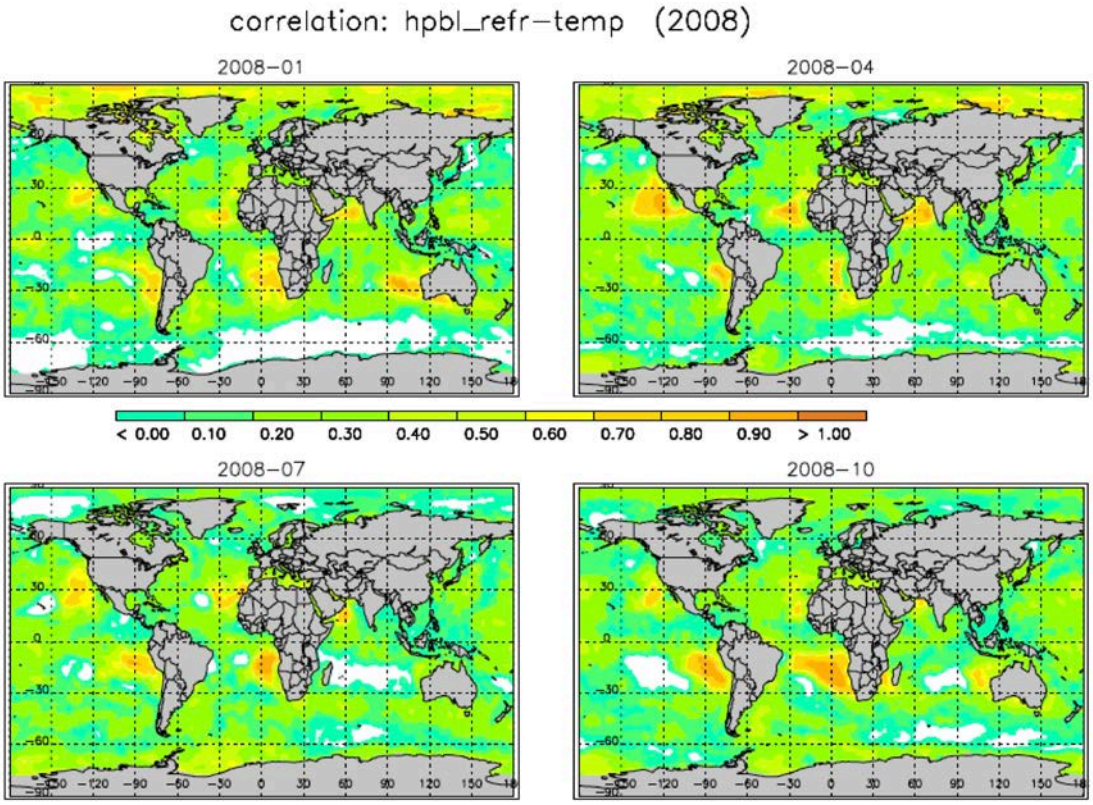


Figure 4.6 Same as Fig. 4.1 but the correlation coefficient between $PBLH_N$ and $PBLH_T$.

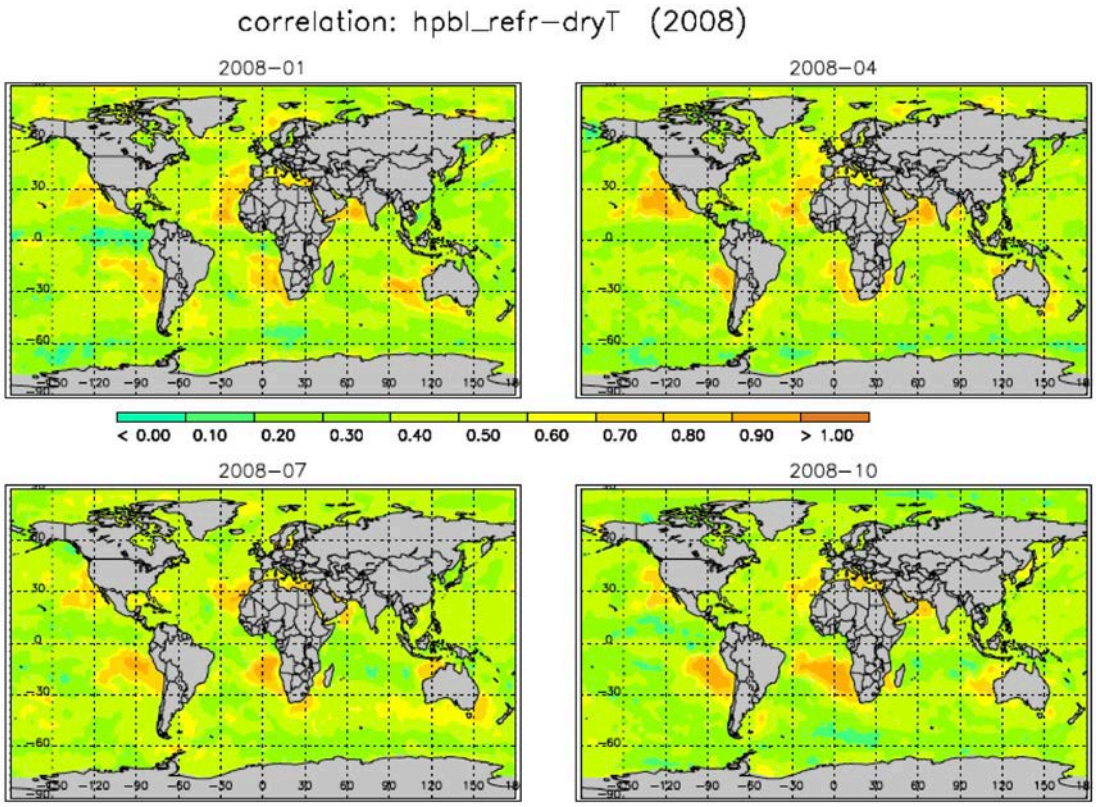


Figure 4.7 Same as Fig. 4.1 but the correlation coefficient between $PBLH_N$ and $PBLH_{Tdry}$.

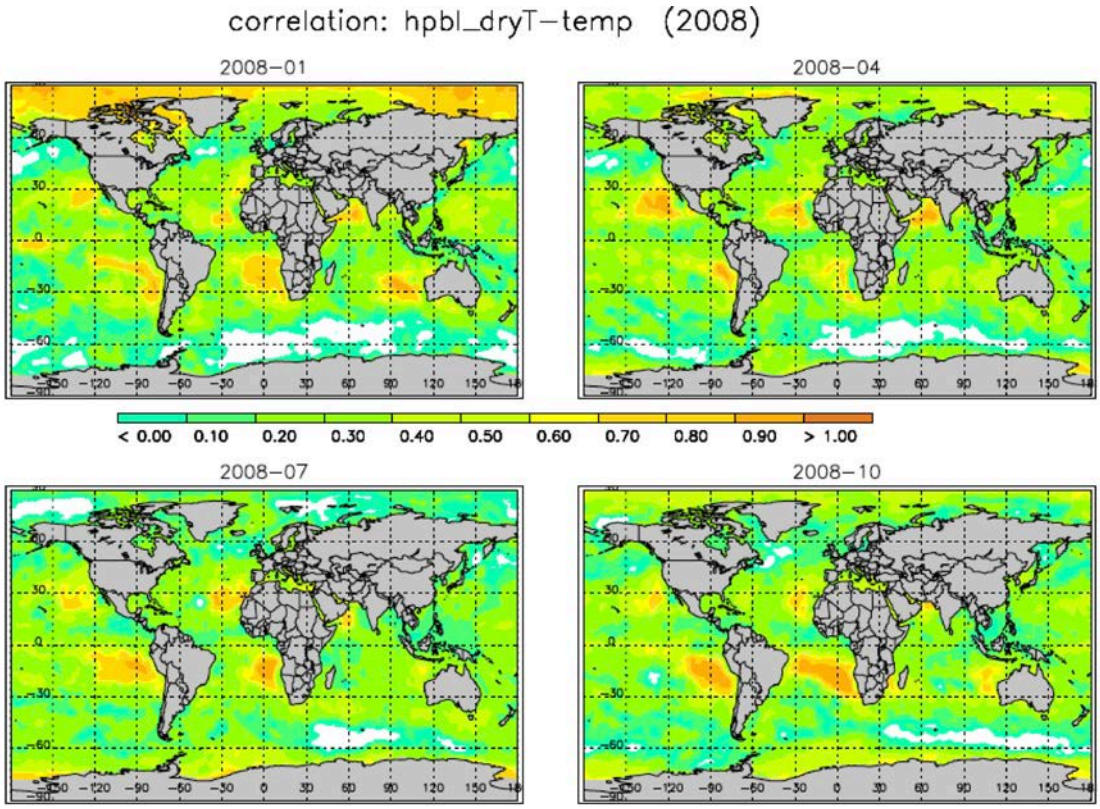


Figure 4.8 Same as Fig. 4.1 but the correlation coefficient between $PBLH_{Tdry}$ and $PBLH_T$.

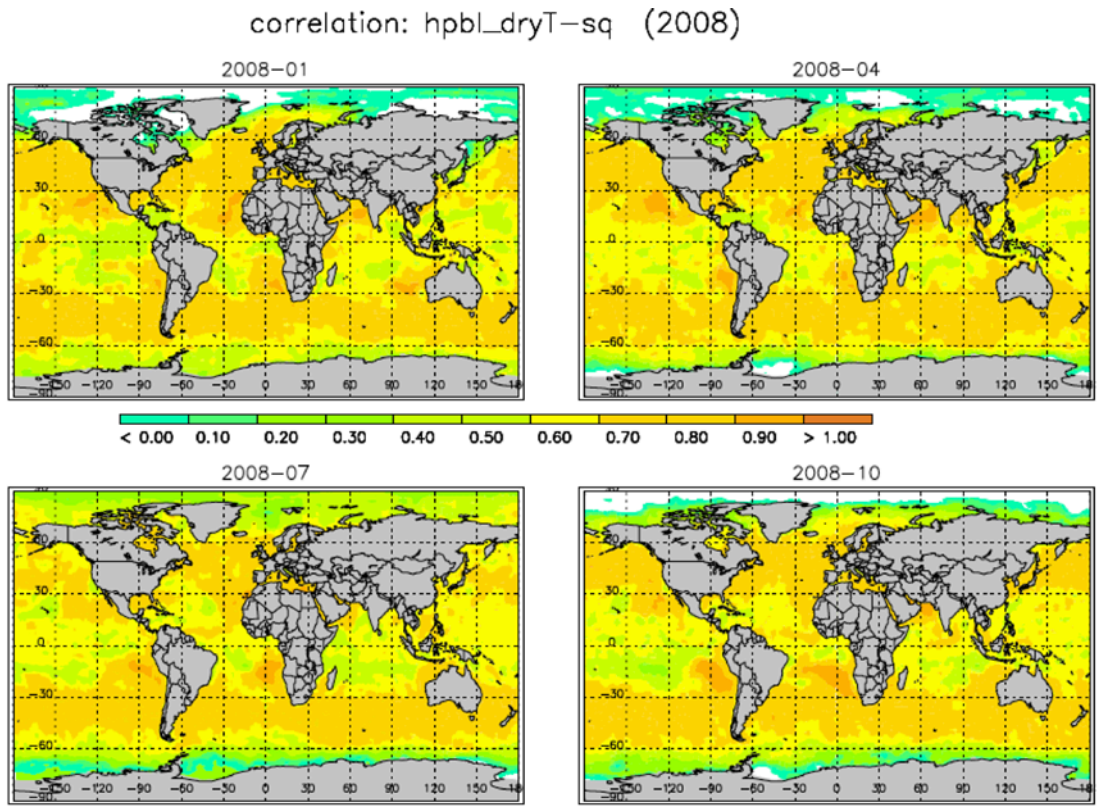


Figure 4.9 Same as Fig. 4.1 but the correlation coefficient between $PBLH_{Tdry}$ and $PBLH_q$.

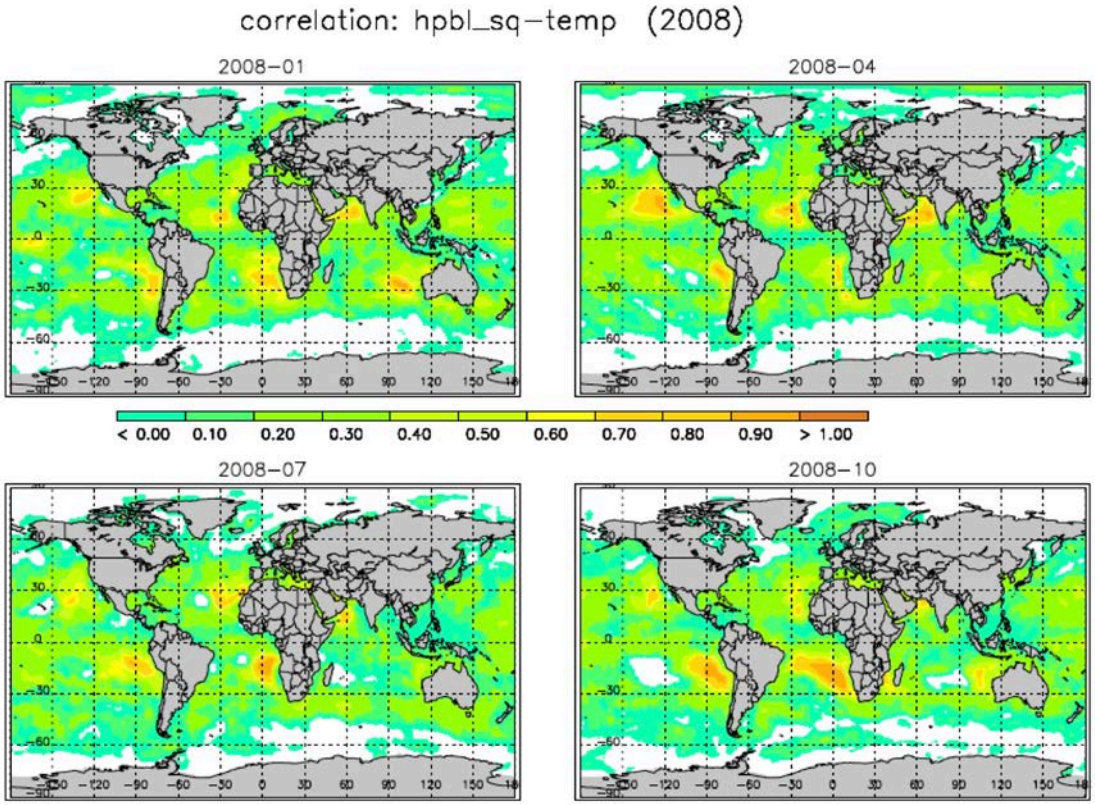


Figure 4.10 Same as Fig. 4.1 but the correlation coefficient between $PBLH_q$ and $PBLH_T$.

## 3.5 PBL vertical structures over selected regions

Significant difference between different PBLH definitions has been shown in Fig. 2.1-2.4. We now look into the vertical profiles over selected regions to understand what is causing the discrepancy among different PBLH definitions. As shown in Figure 5, eight regions are selected based on the large difference between $PBLH_{RH}$ and $PBLH_N$ in 2008-DJF (Fig. 2.1a), except region#5 over southeast Pacific, where minimum difference is found for all PBLH definitions. The eight selected regions include four equatorial/tropical sites (#1-#4), two subtropical sites (#5 and #6) and two polar sites (#7 and #8). The locations of the eight selected boxes and their center grids are listed in Table 2.

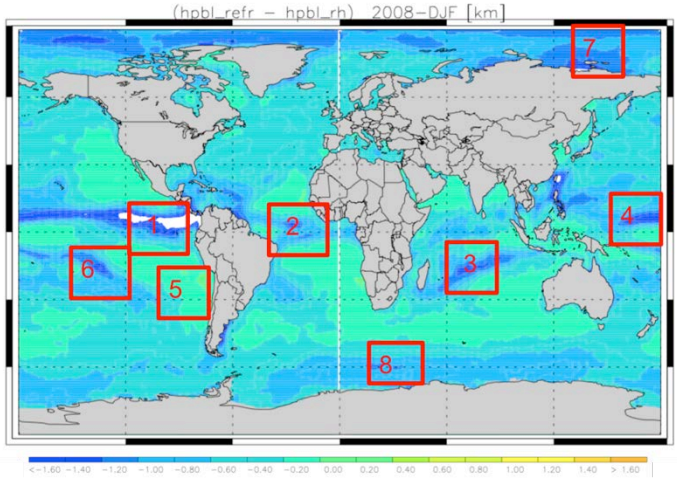


Figure 5 Locations of eight selected regions to study the individual profiles.

Vertical profiles of six parameters (temperature, specific humidity, relative humidity, refractivity, dry temperature and bending angle) are extracted from one hourly file in ERA-i reanalysis at 00Z on January 1, 2008. Individual profiles and their vertical gradients (except bending angle gradients) at the eight selected boxes are displayed in the left and central panels of Figure 6. For better illustration purpose, several parameters and gradient profiles are scaled and horizontally shifted. The thick lines on the central panels are the mean gradient for each parameter. The scatter plot of various PBLH (including bending angle) against $\mathrm{PBLH}_{Tdry}$ in each region is shown on the right panel. Again, the gradient method used in this study will identify the PBLH based on either maximum gradient (e.g., temperature and dry temperature) or minimum gradient (e.g., *RH*, specific humidity, refractivity and bending angle) of an individual profile.

Table 2 Exact locations of vertical profiles from the eight selected regions.

| Region# | 1 | 2 | 3 | 4 | 5 | 6 | 7 | 8 |
|---|---|---|---|---|---|---|---|---|
| Region Names | Equatorial Eastern Pacific | Equatorial Western Atlantic | Equatorial Indian Ocean | Equatorial Western Pacific | Subtropical Southeast Pacific | Subtropical Eastern Pacific | Arctic Ocean | Antarctic southern ocean |
| Latitude Range | [0,10N] | [0,10N] | [10S, 5S] | [0,5N] | [15S,20S] | [15S,10S] | [75N, 85N] | [65S,60S] |
| Longitude Range | [120W, 115W] | [40W, 20W] | [60E,80E] | [150E, 160E] | [100W, 80W] | [160W, 140W] | [110E, 130E] | [20E, 40E] |
| Selected Grid | [5N, 117W] | [2N, 35W] | [7S, 75E] | [2N, 155E] | [17S, 90W] | [12S, 145W] | [80N, 120E] | [62S, 30E] |

In the equatorial eastern Pacific (region#1, in Fig. 6.1a,b), two elevated inversion layers (relatively weak) are seen below 3 km in both temperature and dry temperature profiles. The double-layer structure is clearly seen on the specific humidity, relative humidity and refractivity gradients. Based on the gradient method, the PBL heights based on the mean profiles of five parameters is illustrated as the horizontal bars (Fig. 6.1b). The *RH*, temperature and $T_{dry}$ based PBLH consistently pick up the upper inversion layer. On the contrary, the specific humidity, refractivity and bending angle tend to pick up the lower inversion layer (e.g., clustering in the lower right part of Fig. 6.1c). This phenomenon is also evident in Region#2,3,4&6 for most of the tropical and subtropical regions except the Region#5. This could explain the systematical low (negative) bias in $\mathrm{PBLH}_q$ and $\mathrm{PBLH}_N$

but much less biases in both $PBLH_T$ and $PBLH_{Tdry}$ as compared with $PBLH_{RH}$ over this region in Fig. 2.1.

Note that all the selected tropical and subtropical regions (#1 – #6) also show the presence of a very shallow moist layer right above the surface (e.g., < ~100 m, not shown), which results in a large moisture gradient as clearly seen in all parameters except the temperature. As the elevated PBL is the focus of the study, the algorithms used for all PBLH definitions exclude the lowest 300 m data to avoid picking up this shallow layer.

Also interesting to note that all the tropical and subtropical regions (#1 – #6) show the double-layer PBL structure, the *RH* and dry temperature consistently show larger gradient at the upper layer, whereas the specific humidity and refractivity both tends to have larger gradient at the lower layer. One exception is the region#5 (Fig. 6.5), which represents the subtropical eastern ocean near the major continents. Over this region, a very strong temperature inversion accompanied by a sharp moisture gradient dominate around 1 km. The coexisting temperature and moisture gradients lead to maximum positive (or minimum negative) gradients for all six parameters and result in the most consistent PBLH climatology with difference generally less than ~200 m among six PBLH definitions.

The polar region (Fig. 6.7 – 6.8) shows very dry condition especially in the winter (e.g., near zero specific humidity in Fig. 6a over Arctic winter). Relative humidity also shows large variations in its gradient (Fig. 6.7b) and so the very noisy PBLH (Fig. 6.7c). The large variation of $PBLH_q$ and $PBLH_{RH}$ in Fig. 6.7c indicates that both parameters might not be reliable for PBLH definition in such extremely dry condition. On the other hand, the temperature and dry temperature are consistent to each other and are capable of picking up the weak inversion layer well. The refractivity and bending angle are also capable of resolving the shallow elevated inversion but are also more sensitive to the likely near surface inversion (Fig. 6.7c). It is also interesting to note that during the south polar summer (Fig. 6.8b), a double inversion layer structure is clearly visible, which include a surface inversion and an elevated inversion. The existence of the elevated inversion indicates the likely moist convection process that leads to a shallow mixing layer.

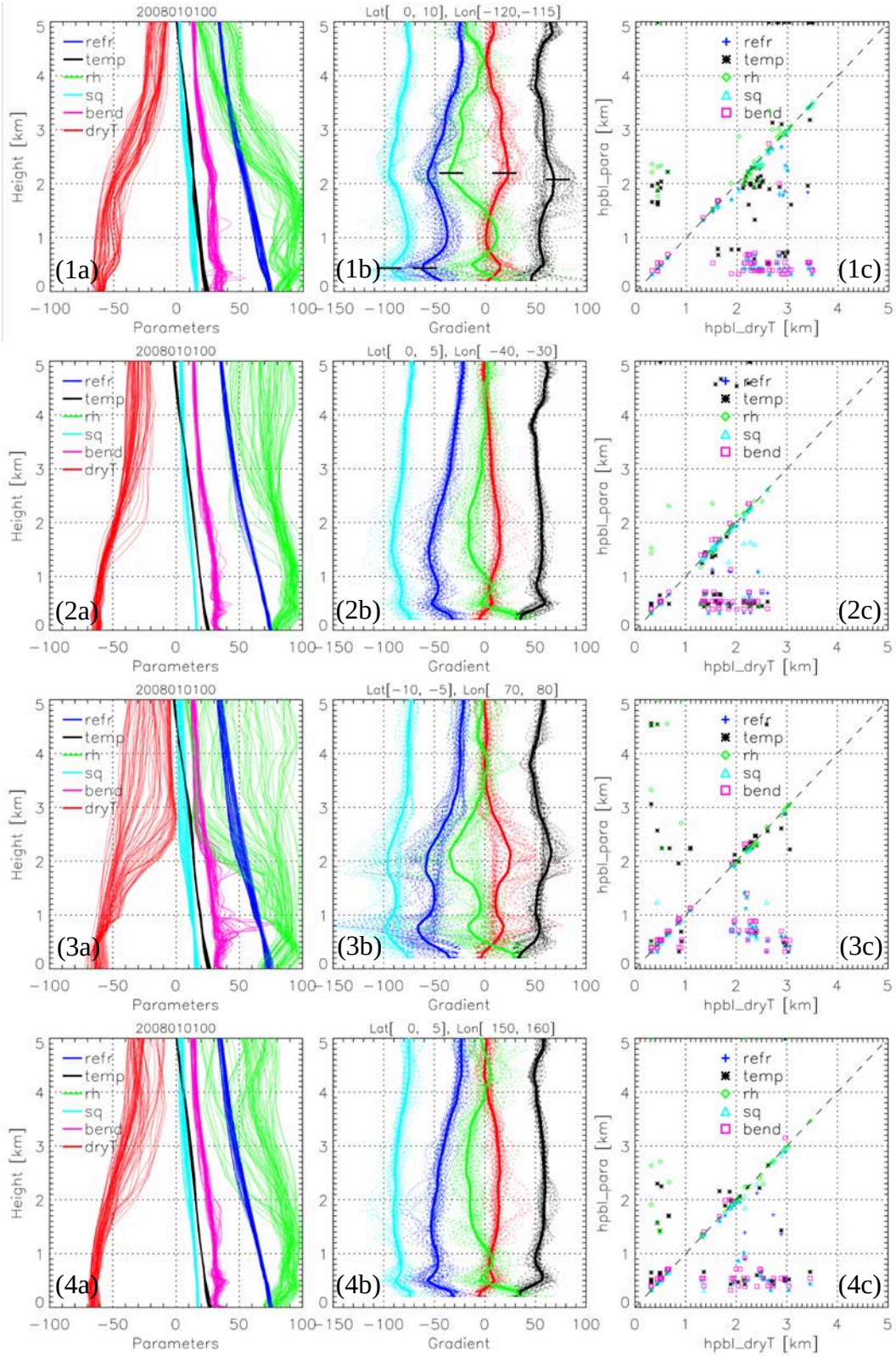
2008010100
Lat[ 0, 10], Lon[-120,-115]
Lat[ 0, 5], Lon[ -40, -30]
Lat[-10, -5], Lon[ 70, 80]
Lat[ 0, 5], Lon[ 150, 160]
refr
temp
rh
sq
bend
dryT
Height [km]
Parameters
Gradient
hpbl_para [km]
hpbl_dryT [km]
(1a)
(1b)
(1c)
(2a)
(2b)
(2c)
(3a)
(3b)
(3c)
(4a)
(4b)
(4c)

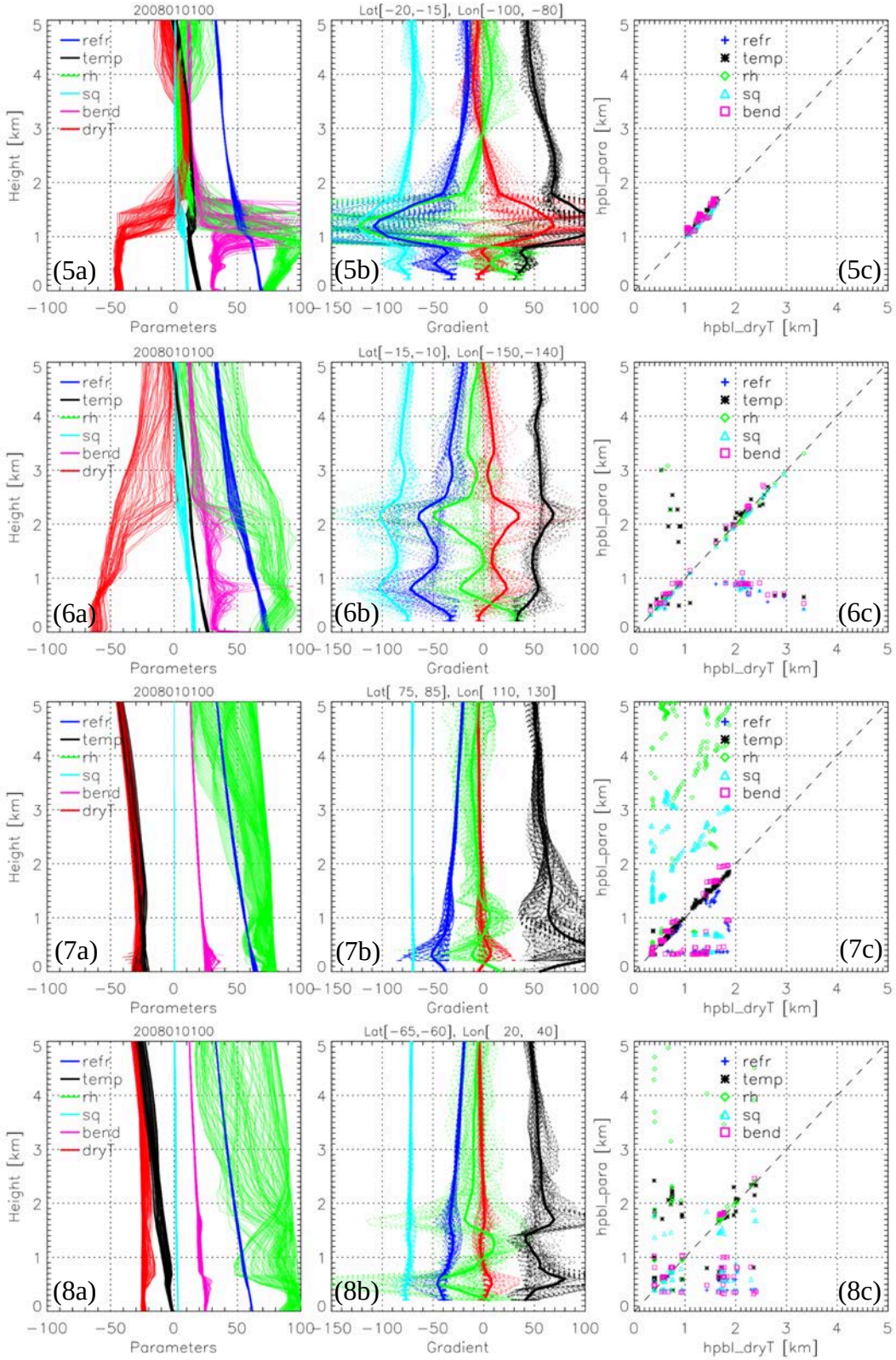


Figure 6 (Left) Vertical profiles from the eight selected regions on 00Z of January 1st, 2008 (Temperature and dry temperature in [K], specific humidity in [g/kg], relative humidity in [%], refractivity (×0.2) in [N-unit] and bending angle (×1000) in [rad]); (middle) vertical gradients of individual profiles (dotted line) and their mean (thick solid). (Temperature gradient (×5+80) in [K/km]; specific humidity gradient (×5-70) in [g/(kg•km)], the five

black horizontal segments in (1b) show the PBLH as indicated by the mean gradient profiles); and (right) scatter plot between $PBLH_{Tdry}$ and the other PBLH definitions for all grid profiles.

Large differences in correlation among various HPBL definitions are demonstrated in Fig. 6 over selected regions, which however are based on only one hourly data. We further study the correlation of different PBLHs within a one-month period. The scatter plots between $PBLH_{RH}$ and other PBLHs at the center grid of each selected regions (Table 2) are shown in Fig. 7. One month of the profiles on January 2008 (e.g., 31 profiles) are analyzed. The correlation of the monthly data further confirms the results shown in Fig. 6. For example, in tropics and subtropics (Region#1-#6), the $PBLH_{Tdry}$ shows very high correlation with $PBLH_{RH}$ ranging from 0.57 in region#3 to 0.98 in region#5. However, over the polar region (Region#7, #8), no significant correlations are found, and the $PBLH_{Tdry}$ shows systematically lower PBLH that is also seen in $PBLH_N$ in both regions and in $PBLH_T$ only during polar winter (e.g., Region#7).

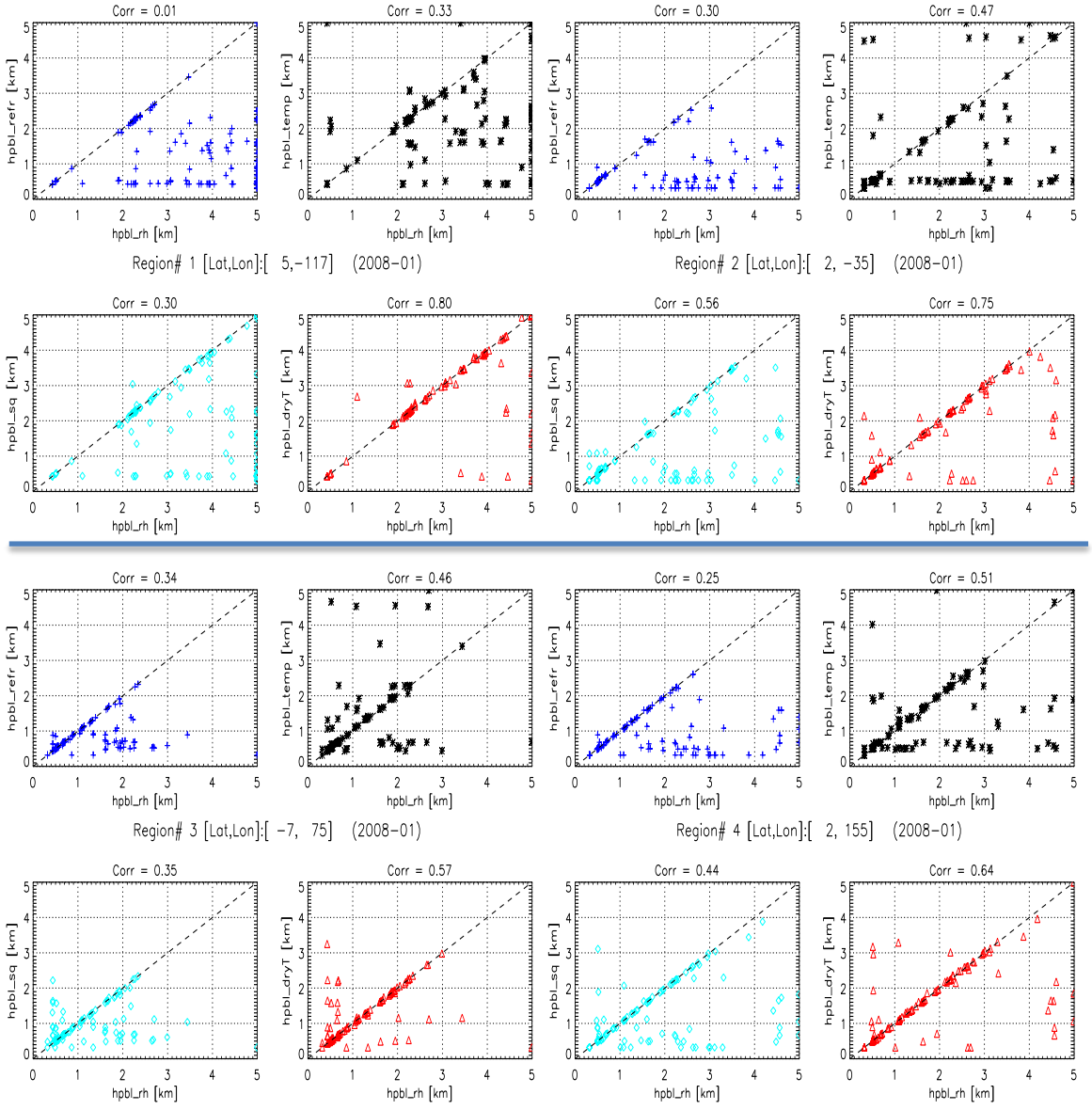

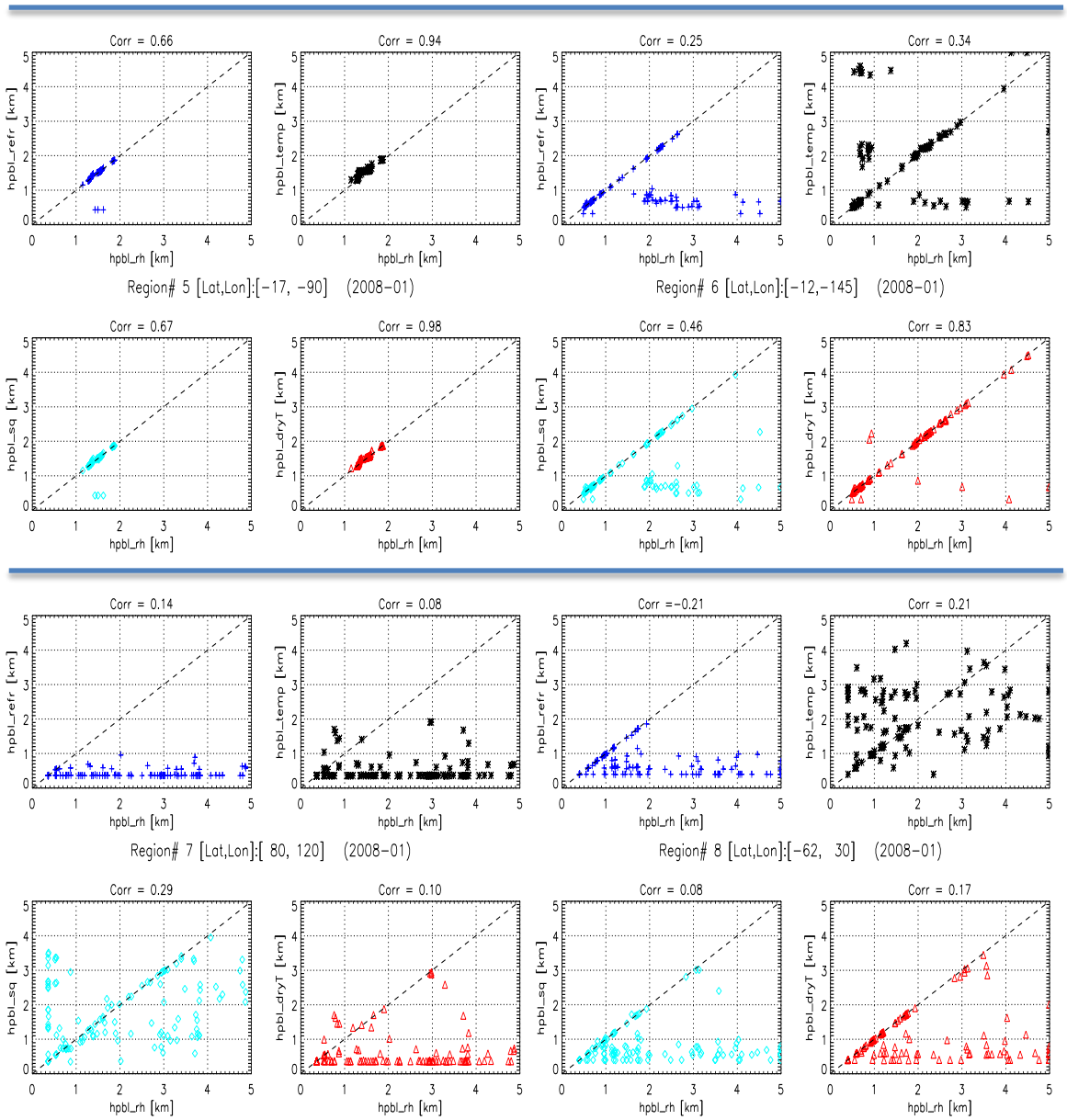


Figure 7 Scatter plots and correlation coefficients of one-month (January, 2008) $PBLH_{RH}$ with four other definitions (refractivity, temperature, specific humidity and dry temperature) at the center grids of the eight selected regions.

# 4. Discussions and Conclusions

The planetary boundary layer height (PBLH) is a fundamental parameter characterizing the vertical extent of atmospheric mixing near the surface. It is critical for understanding the PBL process, which remains a key challenge in both weather and climate modeling. The GPS radio occultation provides high vertical resolution, all-weather global measurements of atmospheric thermodynamic parameters. The direct measurement of GPS RO parameters, such as refractivity, dry temperature and bending angle can be used for global PBLH monitoring.

In this study, the conventional physical parameters (temperature, specific humidity and relative humidity) along with the GPS RO observables (refractivity, dry temperature and bending angle) are obtained from ERA-interim reanalysis. The simple gradient method is applied on the six selected parameters to identify the PBL heights at each grid profiles, respectively. Furthermore, the seasonal climatology of PBLHs over global oceans are derived and compared with each other.

The most dominant features of the seasonal climatology from all PBLH definitions are the dipole structure over the subtropical eastern oceans, with a persistent shallow PBL (~1 km) centered near the west coast of the continents, and a much deeper PBL (~2 km) westward centered at the trade-wind region (e.g., near Hawaii in NE Pacific). These features are clearly seen in both northern and southern Pacific and Atlantic Oceans as well as Southern Indian Ocean in all seasons. The shallow PBL near the west coasts of the continents are consistent with the cool SST due to deep ocean upwelling together with strong subsidence in the free troposphere. The increasing PBL height off shore to a maximum near trade-wind regions is well correlated with the increasing SST and weakening of free troposphere subsidence. In addition, a generally lower PBLH is seen over high latitudes. Notably, the PBLH over the eastern ocean shows the most consistent climatology and highest correlation for all definitions in all seasons. The co-existent strong temperature inversion and sharp moisture gradient result in a dominant gradient in all six parameters and lead to the most consistent PBLH climatology based on the gradient method (e.g., Fig. 5.5c and Fig. 6-Region#5).

Note however, significant difference are found among different definitions. For example, $PBLH_N$ shows rather consistent spatial pattern with the $PBLH_q$ except over polar region. But both show systematic low bias as compared with $PBLH_{RH}$, $PBLH_T$ and $PBLH_{Tdry}$, with the largest negative bias (over 1 km) over tropical ITCZ and subtropical trade-wind regions. $PBLH_N$ also shows most consistent with $PBLH_\alpha$ (e.g., Fig. 6).

The $PBLH_T$ shows rather consistent spatial pattern and relative high correlation with $PBLH_{RH}$ over subtropics and mid latitude. But some systematic negative biases are concentrated over tropics and high latitudes.

Interestingly, the $PBLH_{Tdry}$ shows high consistence and high correlation with the $PBLH_{RH}$ from tropics to the mid-latitude (Figs. 2-3). Note however, $PBLH_{Tdry}$ shows systematic lower PBL over polar region especially over winter Arctic Ocean. The low biases are also seen in $PBLH_T$ and $PBLH_N$, which indicate the potential of overestimate of $PBLH_{RH}$ during

extremely dry polar winter (Fig. 6.7c). $PBLH_{Tdry}$ and $PBLH_{T}$ show very consistent pattern with $PBLH_{RH}$ at all seasons except the polar region.

Selected regional analysis indicates high frequency of double elevated gradient layers (in both temperature and humidity) below 3 km from tropics, subtropics to mid-latitude and polar summer (e.g., Figs. 6.1-6 & 8). The gradient of refractivity, bending angle and specific humidity are generally more sensitive to the shallower mixing layer (below 800m with relative weak inversion and slightly stronger moisture gradient) over equatorial and subtropical trade-wind regions, whereas the *RH* and $T_{dry}$ gradients are more sensitive to the higher inversion layer (e.g., stronger inversion but likely comparable or less moisture gradient).

In general, both the specific humidity and relative humidity should be avoided over polar winter due to very low water vapor concentration that could lead to large uncertainty in PBLH detection. An ideal absolute humidity threshold need to be developed to guide the applicability of the *RH*/q based PBLH usage over dry regions (including subtropical deserts and polar region in winter season).

This study demonstrates the great promise of using GPS RO observables (especially the dry temperature) for global PBLH sensing. However, it is important to note that to derive the PBLH from the real GPS RO measurements, several issues need to be carefully addressed. Several recommendations are as follows:

1) Derive $PBLH_{Tdry}$.

   ***GPS RO dry temperature*** seems to be the most favorable RO parameter for global PBLH characterization over the oceans. It has the advantage of being a model-independent RO observable that is sensitive to both temperature and humidity along with the global applicability from moist tropics to dry polar region as indicated by this study. Moreover, it has a simple relation with the conventional atmospheric parameters such as temperature, humidity and pressure.

   Note that in the GPS RO retrieval, the dry temperature is derived from the RO refractivity along with the hydrostatic pressure (referred to as dry pressure, without including the moisture partial pressure). In the project, we simply use the total pressure and refractivity to derive the dry temperature, which could lead to a small positive bias in absolute dry temperature but should not affect much of the altitude of the maximum vertical gradient (i.e., the $PBLH_{Tdry}$). However, it could be interesting to assess such impact in more details.

   ***Other PBLH products***: GPS RO refractivity and bending angle are also valuable and especially for regional studies. For example, the bending angle could potentially provide best sensitivity to the sharp change of temperature or moisture gradients (when exits, e.g. over subtropical eastern oceans) leading to highest precision of the PBLH.

2) Develop robust PBLH detection algorithms.

In this project, the ERA-interim reanalysis provides rather smooth vertical profiles with uniform vertical resolution, which makes the gradient method easily applicable. Much more robust detection algorithms are necessary to handle the noisy GPS RO profiles.

***Optimal smoothing***: The gradient method is sensitive to both the vertical sampling interval of the RO profiles as well as noise structure. Current GPS RO retrieval generally apply ~200-m vertical smoothing on the bending angle to reduce the noise, which tend to smooth out the fine structure near the PBL top. An optimal smoothing method needs to be explored to preserve the fine vertical structures of the RO observables, which will lead to higher precision of PBLH.

***Gradient thresholds***: Due to the different sensitivity of RO observables (bending, refractivity and dry temperature) to temperature and humidity gradients across the PBL top, individual thresholds need to be quantified to allow precise detection of PBLH for each RO observable. Such thresholds (e.g., gradient and altitude ranges, etc.) might even exhibit spatial and temporal variations.

3) Quantify the sampling bias of GPS RO.

***Spatial sampling errors***: Current GPS RO satellites (e.g., COSMIC) provide denser sampling per unit area in middle latitude and polar region than in the tropics (Xie et al., 2012). The potential sampling errors due to the uneven sampling especially in the meridional direction need to be considered when compiling the PBLH climatology at different temporal scale (e.g., diurnal, monthly, seasonal etc.).

***Vertical sampling/Uneven penetration issue***: In addition, not all the RO profiles penetrate deep into the PBL. The percentage of RO that penetrate into the lowest 500 m in PBL tends to be lower in the tropics than in higher latitudes. For example, only about 20%-30% RO profiles penetrate deep into the lowest 500m above mean sea level near equator (0-10°S), whereas the penetration rate increases at higher latitude and reach over 60% at ~50°S (Xie et al., 2012). The limited penetration depth could result in missing capture of the shallow mixing layer in low latitudes and surface inversion over high latitudes and result in a positive bias in PBLH climatology.

4) Offer high quality GPS RO PBL profiles.

In addition to offer the PBLH observations, GPS RO also provides global sounding of high vertical resolution thermodynamic structure of the atmosphere from the PBL, throughout the free troposphere up to the stratosphere. Development of high-quality RO PBL sounding profiles could be even more valuable for PBL studies. However, additional quality control will be necessary.

***Ducting impact***: the impact of the ducting on the GPS RO observables and so the PBLH detection requires further study. The radiosondes and the global analyses and reanalyses confirm the prevalence of a ducting layer at the PBL top over subtropical eastern oceans (von Engeln and Teixeira, 2004; Lopez, 2009; Xie et al., 2012). Ducting leads to systematic negative bias and so reduced gradients in refractivity (Sokolovskiy, 2003, Xie et al., 2006, Ao, 2007, Xie et al., 2010), and dry temperature retrievals,

which also leads to a smaller bending angle. Xie et al. (2012) demonstrated the consistent PBLH detection from COSMIC as compared with near coincident radiosondes in the presence of ducting over southeast Pacific. However, the impact of the reduced vertical gradients as results of ducting on the PBLH detection in the other regions warrants further investigation.

***Penetration issue***: the uneven penetration of RO profiles into the PBL also require further attention, as it limits the capability of GPS RO to detect the shallow mixing layer or surface inversion layer that are often observed over polar region.

***PBLH over land and horizontal inhomogeneity impact***: The PBL over land is important for air pollution and wind energy studies. It is reasonable to believe that the GPS RO will provide the same or similar quality PBL profiles over land as that over oceans, since the GPS RO retrieval is not affected by the surface property. However, the much larger surface heating difference due to the variation of topography and surface types over land could lead to larger horizontal inhomogeneous structures inside the PBL. The horizontal atmospheric structure impact on GPS RO retrieval will need to be quantified, which will improve understanding the quality of RO PBL profiles and their PBLH products..

## 4.1 User applications

This project demonstrates that the GPS RO observables are well suited for global PBLH detection due to their sensitive to both water vapor and temperature gradients that generally mark the PBLH. The global PBLH product derived from GPS RO measurements will provide essential observational constraints in several research areas. (1) Provide benchmark PBLH observations for evaluating the PBL parameterization in weather and climate models. (2) Improve understanding physical processes inside the PBL, including the shallow convection, low cloud evolutions and turbulence mixing etc. (3) Advance atmospheric transport model development and improve regional or global air pollution simulation and forecasting. (4) Help constrain high-resolution regional weather model and benefit wind energy planning and development.

# Acknowledgments

I would like to thank Drs. Stig Syndergaard and Kent B. Lauritsen (DMI) for making it possible to perform this visiting scientist activity. Especially I am grateful to Stig Syndergaard for his support and help. I would also like to extend my appreciation to Drs. Axel von Engeln (EUMETSAT) and Ian Culverwell (UK Met Office) for very fruitful, motivating and encouraging discussions and providing the ERA-i reanalysis data.

# List of Acronyms

| | |
|---|---|
| COSMIC | Constellation Observing System for Meteorology, Ionosphere, and Climate |
| ECMWF | European Centre for Medium-range Weather Forecasts |
| EUMETSAT | EUropean organisation for the exploitation of METeorological SATellites |
| GNSS | Global Navigation Satellite System |
| GPS | Global Positioning System (USA) |
| GRAS | GNSS Receiver for Atmospheric Sounding (on Metop) |
| Metop | Meteorological Operational Satellite |
| NWP | Numerical Weather Prediction |
| PBL | Planetary Boundary Layer |
| PBLH | Planetary Boundary Layer Height |
| $PBLH_{\alpha}$ | Planetary Boundary Layer Height based on bending angle |
| $PBLH_{N}$ | Planetary Boundary Layer Height based on refractivity |
| $PBLH_{q}$ | Planetary Boundary Layer Height based on specific humidity |
| $PBLH_{RH}$ | Planetary Boundary Layer Height based on relative humidity |
| $PBLH_{Tdry}$ | Planetary Boundary Layer Height based on dry temperature |
| RH | Relative Humidity |
| RO | Radio Occultation |
| ROM SAF | Radio Occultation Meteorology (ROM) Satellite Application Facility (SAF) (EUMETSAT) |
| T*dry* | Dry Temperature |

# List of Figures

Figure 6 (Left) Vertical profiles from the eight selected regions on 00Z of January 1st, 2008 (Temperature and dry temperature in [K], specific humidity in [g/kg], relative humidity in [%], refractivity (×0.2) in [N-unit] and bending angle (×1000) in [rad]); (middle) vertical gradients of individual profiles (dotted line) and their mean (thick solid). (Temperature gradient (×5+80) in [K/km]; specific humidity gradient (×5-70) in [g/(kg•km)], the five black horizontal segments in (1b) show the PBLH as indicated by the mean gradient profiles); and (right) scatter plot between $PBLH_{Tdry}$ and the other PBLH definitions for all grid profiles.

Figure 7 Scatter plots and correlation coefficients of one-month (January, 2008) $PBLH_{RH}$ with four other definitions (refractivity, temperature, specific humidity and dry temperature) at the center grids of the eight selected regions.

# List of Tables

# References

Anthes, R. A. and Coauthors: The COSMIC/FORMOSAT-3 mission: Early results, Bull. Am. Meteorol. Soc., 89, 313–333, 2008.

Ao, C. O., Meehan, T. K., Hajj, G. A., Mannucci, A. J., and Beyerle, G.: Lower-troposphere refractivity bias in GPS occultation retrievals. J. Geophys. Res., 108, doi:10.1029/2002JD003216, 2003.

Ao, C. O.: Effect of ducting on radio occultation measurements: An assessment based on high-resolution radiosonde soundings, Radio Sci., 42, RS2008, doi:10.1029/2006RS003485, 2007.

Ao, C. O., Hajj, G. A., Meehan, T. K., Dong, D., Iijima, B. A., Mannucci, A. J., and Kursinski, E. R.: Rising and setting GPS occultations by use of open-loop tracking, J. Geophys. Res., 114, D04101, doi:10.1029/2008JD010483, 2009.

Ao, C. O., Chan, T. K., Iijima, B. A., Li, J.-L., Mannucci, A.J., Teixeira, T., Tian, B., and Waliser, D. E.: Planetary boundary layer information from GPS radio occultation measurements, ECMWF GRAS SAF Workshop on Applicaitons of GPS Radio Occultation Measurements (16 - 18 June 2008), Reading, UK, pp. 123-131, 2008.

Ao, C. O., D. E. Waliser, S. K. Chan, J.-L. Li, B. Tian, F. Xie, and A. J. Mannucci, 2012, Planetary boundary layer depths from GPS radio occultation profiles, *J. Geophys. Res.*, 117, D16117, doi:10.1029/2012JD017598.

Basha, G., and Ratnam, M. V.: Identification of atmospheric boundary layer height over a tropical station using high resolution radiosonde refractivity profiles: Comparison with GPS radio occultation measurements, J. Geophys. Res., 114, D16101, doi:10.1029/2008JD011692, 2009.

Beyerle, G., Schmidt, T., Wickert, J., Heise, S., Rothacher, M., Ko¨nig-Langlo, G., and Lauritsen, K. B.: Observations and simulations of receiver-induced refractivity biases in GPS radio occultation, J. Geophys. Res., 111, D12101, doi:10.1029/2005JD006673, 2006.

Bony, S., and Dufresne J.-L.: Marine boundary layer clouds at the heart of tropical cloud feedback uncertainties in climate models, Geophys. Res. Lett., 32, L20806, doi:10.1029/2005GL023851, 2005.

Bretherton, C. S., et al.: The EPIC 2001 stratocumulus study, Bull. Am. Meteorol. Soc., 85, 967–977, doi:10.1175/BAMS-85-7-967, 2004.

Bretherton, C. S., Wood, R., George, R. C., Leon, D., Allen, G. and Zheng X.: Southeast Pacific stratocumulus clouds, precipitation and boundary layer structure sampled along 20S during VOCALS-Rex, Atmos. Chem. Phys., 10, 10639–10654, doi:10.5194/acp-10-10639-2010, 2010.

Clement, A. C., Burgman R., and Norris J. R.: Observational and model evidence for positive low-level cloud feedback. Science, 325, 460-464, DOI: 10.1126/science.1171255, 2009.

Duynkerke, P.G. and J. Teixeira, 2001: Comparison of the ECMWF Reanalysis with FIRE I observations: diurnal variation of marine stratocumulus. Journal of Climate, 14, 1466-1478.

Fjeldbo G., Kliore, A. J., and Eshleman, V. R.: The neutral atmosphere of Venus as studied with the Mariner V radio occultation experiment. Astron. J., 76, 123–140, 1971.

Garratt, J. R.: The atmospheric boundary layer, Cambridge University Press, 316pp., 1992.

Guo, P., Y.-H. Kuo, S. Sokolovskiy, and D. Lenschow, Estimating atmospheric boundary layer depth using COSMIC radio occultation data, *J. Atmos. Sci.*, **68(8)**, 1703-1713, doi:10.1175/2011JAS3612.1, 2011.

Hajj, G. A., Kursinski, E. R., Romans, L. J., Bertiger, W. I., and Leroy, S. S.: A technical description of atmospheric sounding by GPS occultation. J. Atmos. Solar Terr. Phys., 64, 451– 469, 2002.

Healy, S.B. and Eyre, J.R.: Retrieving temperature, water vapour and surface pressure information from refractivity-index profiles derived by radio occultation: A simulation study. Q. J. R. Meteorol. Soc., 126, 1661-1683, 2000.

Kursinski, E. R., Hajj, G. A., Schofield, J. T., Linfield, R. P., and Hardy, K. R.: Observing Earth's atmosphere with radio occultation measurements using the Global Positioning System, J. Geophys. Res., 102, 23429-23465, 1997.

Kursinski, E. R., G. A. Hajj, S. S. Leroy, and B. Herman, 2000: The GPS radio occultation technique. *Terr. Atmos. Oceanic Sci.,* **11,** 53–114.

Lopez P.: A 5-yr 40-km-Resolution Global Climatology of Superrefraction for Ground-Based Weather Radars. J Appl. Meteorol. Clim., 48(1), 89-110, 2009.

Rocken, C., and Coauthors: Analysis and validation of GPS/MET data in the neutral atmosphere. *J. Geophys. Res.*, **102,** 29 849–29 866, 1997.

Seidel D., Ao, C. O., and Li, K.: Estimating climatological planetary boundary layer heights from radiosonde observations: Comparison of methods and uncertainty analysis, J. Geophys. Res., doi:10.1029/2009JD013680, 2010.

Smith, E. K., and Weintraub, S.: The constants in the equation for atmospheric refractive index at radio frequencies, Proc. Inst. Radio Engrs., 41, 1035-1037, 1953.

Soden B. J. and Held I. M.: An Assessment of Climate Feedbacks in Coupled Ocean–Atmosphere Models. J. Climate, 19, 3354–3360, 2006.

Sokolovskiy, S. V.: Tracking tropospheric radio occultation signals from low Earth orbit. Radio Sci., 36, 483–498, 2001.

Sokolovskiy, S. V.: Effect of superrefraction on inversions of radio occultation signals in the lower troposphere. Radio Sci., 38, 1058, doi:10.1029/2002RS002728, 2003.

Sokolovskiy, S., Kuo, Y.-H., Rocken, C., Schreiner, W. S., Hunt, D., and Anthes, R. A.: Monitoring the atmospheric boundary layer by GPS radio occultation signals recorded in the open-loop mode, Geophys. Res. Lett., 33, L12813, doi:10.1029/2006GL025955, 2006.

Sokolovskiy, S. V., Rocken, C., Lenschow, D. H., Kuo, Y.-H., Anthes, R. A., Schreiner, W. S. and Hunt, D. C.: Observing the moist troposphere with radio occultation signals from COSMIC, Geophys. Res. Lett., 34, L18802, doi:10.1029/2007GL030458, 2007.

Stephens, G. L.: Cloud Feedbacks in the Climate System: A Critical Review. *J. Climate*, **18**, 237–273. doi: http://dx.doi.org/10.1175/JCLI-3243.1, 2005.

Teixeira, J. et al., 2011: Tropical and sub-tropical cloud transitions in weather and climate prediction models: the GCSS/WGNE Pacific Crosssection Intercomparison (GPCI). J. Climate, 24 (20), 5223{5256, doi:10.1175/2011JCLI3672.1.

Tjernström and Graversen: The vertical structure of the lower Arctic troposphere analysed from observations and the ERA-40 reanalysis. Q J R Meteorol Soc 135:431–443, 2009.

von Engeln, A., and Teixeira, J.: A ducting climatology derived from the European Centre for Medium-Range Weather Forecasts global analysis fields. J. Geophys. Res., 109, D18104, doi:10.1029/2003JD004380, 2004.

von Engeln, A., J. Teixeira, J. Wickert, and S. A. Buehler: Using CHAMP radio occultation data to determine the top altitude of the Planetary Boundary Layer, Geophys. Res. Lett., 32, L06815, doi:10.1029/2004GL022168, 2005.

von Engeln, A., J. Teixeira, 2013: A Planetary Boundary Layer Height Climatology Derived from ECMWF Reanalysis Data. *J. Climate*, **26**, 6575–6590. doi: http://dx.doi.org/10.1175/JCLI-D-12-00385.1

Wood, R. and Coauthors: The VAMOS Ocean-Cloud-Atmosphere-Land Study Regional Experiment (VOCALS-REx): goals, platforms, and field operations. Atmos. Chem. Phys., 11, 627–654, doi:10.5194/acp-11-627-2011, 2011.

Wyant, M. C., M. Khairoutdinov, and C. S. Bretherton: Climate sensitivity and cloud response of a GCM with a superparameterization. Geophys. Res. Lett., 33, L06714, doi: 10.1029/2005GL025464, 2006.

Wyant, M. C., Wood, R., Bretherton, C. S., Mechoso, C. R., Bacmeister, J., Balmaseda, M. A., Barrett, B., Codron, F., Earnshaw, P., Fast, J., Hannay, C., Kaiser, J. W., Kitagawa, H., Klein, S. A., Köhler, M., Manganello, J., Pan, H.-L., Sun, F., Wang, S., and Wang, Y.: The PreVOCA experiment: modeling the lower troposphere in

the Southeast Pacific, Atmos. Chem. Phys., 10, 4757-4774, doi:10.5194/acp-10-4757-2010, 2010.

Xie F.: Development of a GPS Occultation Retrieval Method for Characterizing the Marine Boundary Layer in the Presence of Super-refraction, Dissertation, University of Arizona, 134pp, 2006.

Xie, F., Syndergaard, S., Kursinski, E. R., and Herman, B. M.: An Approach for Retrieving Marine Boundary Layer Refractivity from GPS Occultation Data in the Presence of Super-refraction, J. Atmos. Ocean Tech, 23, 1629-1644, 2006.

Xie, F., Wu, D. L., Ao, C. O., Kursinski, E. R., Mannucci, A. and Syndergaard, S.: Super-refraction effects on GPS radio occultation refractivity in marine boundary layers, Geophys. Res. Lett., 37, L11805, doi:10.1029/2010GL043299, 2010.

Xie, F., Wu, D. L., Ao, C. O., Mannucci, A. J., and Kursinski, E. R.: Advances and limitations of atmospheric boundary layer observations with GPS occultation over southeast Pacific Ocean, Atmos. Chem. Phys., 12, 903-918, doi:10.5194/acp-12-903-2012, 2012.

Zou, X., Y.-H. Kuo, and Y.-R. Guo: Assimilation of atmospheric radio refractivity using a nonhydrostatic mesoscale model, Mon. Wea. Rev., 123, 2229-2249, 1995.